HHS Public Access

Author manuscript

J Immunol. Author manuscript; available in PMC 2020 February 01.

Published in final edited form as:

J Immunol. 2019 February 01; 202(3): 883–898. doi:10.4049/jimmunol.1801101.

ATP-gated P2X7 receptors require chloride channels to promote inflammation in human macrophages

Laura Janks, **Randy S. Sprague**, and **Terrance M. Egan***

Department of Pharmacology and Physiology, Saint Louis University School of Medicine, St. Louis, Missouri, USA.

Abstract

Immune cells of myeloid origin show robust expression of ATP-gated P2X7 receptors, two-transmembrane ion channels permeable to Na^+, K^+, and Ca^{2+}. Receptor activation promotes inflammasome activation and release of the proinflammatory cytokines IL-1β and IL-18. Here, we show that ATP generates facilitating cationic currents in monocyte-derived human macrophages and permeabilizes the plasma membrane to polyatomic cationic dyes. We find that antagonists of phospholipase A2 and Cl^- channels abolish P2X7 receptor-mediated current facilitation, membrane permeabilization, blebbing, phospholipid scrambling, inflammasome activation, and IL-1β release. Our data demonstrate significant differences in the actions of ATP in murine and human macrophages, and suggest that phospholipase A2 and Cl^- channels mediate innate immunity downstream of the P2X7 receptors in human macrophages.

Keywords

ligand-gated ion channel; purinergic receptor; permeabilization; dye uptake; inflammation; innate immunity; IL-1β; inflammasome; PLA_2; Cl^- channel; phospholipid scrambling; membrane blebbing; reactive oxygen species

Introduction

The P2X7 receptor, a member of the P2 family of nucleotide receptors (P2X1R-P2X7R), regulates critical macrophage inflammatory functions including cell fusion, intracellular bacterial killing, cytokine release, and apoptosis (1–4). P2X7Rs form non-selective cation channels permeable to Na^+, K^+, and Ca^{2+} that open upon binding extracellular adenosine 5′-triphosphate (ATP) or the synthetic agonist 3′-*O*-(4-benzoylbenzoyl) ATP (BzATP) (5). Human P2X7Rs are relatively insensitive to ATP and thus inactive in healthy tissues, but activate following tissue injury when the concentration of ATP in the interstitial fluid rises to several hundred micromolar (6, 7). Here, ATP acts as a damage-associated molecular pattern

*To whom correspondence should be addressed: Terrance M. Egan, Ph.D., Department of Pharmacology and Physiology, Saint Louis University School of Medicine, 1402 South Grand Bofigulevard, St. Louis, Missouri 63104, USA; *Telephone*, 314-977-6429; *FAX*, 314-977-6411; terrance.egan@health.slu.edu.

Author contributions: Isolation of monocytes from human blood (L.J., R.S. and T.M.E.); YO-PRO-1 uptake time-course (T.M.E.); all other procedures and experiments (L.J.); experimental design and data analysis (L.J. and T.M.E.); first draft of the paper (L.J.); final draft of paper (L.J., R.S., T.M.E.).

Competing Interests: The authors declare no competing interests.

that initiates a non-infectious innate immune response (8). In the presence of a bacterial infection, endotoxins sensitize phagocytes to the actions of ATP so that far lower concentrations are sufficient to fully activate P2X7Rs (9). Furthermore, P2X7Rs are activated by molecular patterns other than ATP, including the coenzyme nicotinamide adenine dinucleotide (10, 11), the amyloidogenic 1–42 β-amyloid peptide (12), the acute-phase protein serum amyloid (13), the bactericidal peptide cathelicidin LL-37 (14, 15), and repetitive Alu-derived RNAs (16, 17). Like ATP, these newly identified ligands accumulate at inflammatory foci, suggesting that P2X7Rs play a prominent role in sensing a diverse range of inflammatory mediators.

Activation of P2X7Rs stimulate several pro-inflammatory pathways in murine leukocytes. First, they promote assembly of the NLRP3 inflammasome, a multiprotein intracellular pattern recognition receptor that mediates caspase-1 maturation (18). Caspase-1 in turn cleaves inactive pro-IL-1β and pro-IL-18 into their operational forms, and frees the biologically active N-terminal domain of Gasdermin D from the full-length protein (19). The N-terminal domain of Gasdermin D localizes to the plasma membrane (20), where it forms transmembrane pores through which the proinflammatory cytokine, IL-1β, exits the cell (21). Second, P2X7Rs regulate macrophage exocytosis, migration, and changes in cell morphology (22). Activation of P2X7Rs causes extensive membrane blebbing, which is linked to reversible disruption of the cytoskeleton and stimulation of p38 MAPK and Rho G-proteins (23, 24). Third, P2X7Rs trigger phosphatidylserine (PS) exposure on the outer leaflet of the plasma membrane of lymphocytes (25), erythrocytes (26), and thymocytes (27), which serves as an apoptotic “eat me” signal (28, 29). Importantly, blebbing and PS flip are fully reversible events that do not lead to death when cells are exposed to ATP for less than 30 mins. Longer activation of the P2X7R triggers release of mitochondrial cytochrome *c*, signaling cell demise (30).

Persistent stimulation of the P2X7R also promotes increased membrane permeability which allows the cellular uptake of large molecular weight fluorescent dyes (31, 32). This increased permeability is linked to facilitation of P2X7R currents (33) and several other physiological functions such as inflammasome activation (34, 35), inhibition of phagocytosis (36), activation of p38 MAPK (37, 38), and the production of nitrites and reactive oxygen species (ROS) (39). Sustained activation of the dye uptake pathway ultimately leads to cytolysis (40) and apoptotic cell death (30).

Given the abundant evidence in support of the P2X7R as a central driver of inflammation in rodents, a crucial next step is to identify the downstream signaling molecules required for activating these inflammatory pathways in humans, which may lead to a better understanding of how the P2X7R initiates such a diverse range of signaling cascades. In the present study, we investigated the mechanism by which the P2X7R modulates inflammatory processes in primary human macrophages derived from circulating monocytes. Here we report for the first time that some of the most important effects of P2X7Rs on innate immune function (membrane permeabilization and blebbing, PS exposure, caspase-1 activation, and IL-1β release) are blocked by pharmacological inhibitors of phospholipase A2 (PLA_2) and Cl^- channels. We propose that P2X7Rs stimulate PLA_2 which in turn activates Cl^- channel mediated inflammation in human macrophages.

Materials and Methods

Materials

RPMI 1640, penicillin and streptomycin were purchased from Gibco by Life Technologies (Waltham, MA, USA). ATP, BzATP, EDTA, lipopolysaccharides from E. coli O55:B5 (LPS; L2880), dimethyl sulfoxide (DMSO), Na gluconate, K gluconate, Lucifer yellow dilithium salt, 5 (6)-carboxyfluorescein, cabenoxolone, tannic acid, 4,4'-Diisothiocyano-2,2'-stilbenedisulfonic acid (DIDS), CaCCinh-A01 (A01), 5-Nitro-2-(3-phenylpropylamino)benzoic acid (NPPB), nigericin, ionomycin, MCC950, and Melittin (MEL) were purchased from Millipore Sigma (St. Louis, MO, USA). MQAE, BAPTA-AM, YO-PRO-1, YOYO-1, pHrodo Red *E. coli* BioParticles Conjugate, and 35 mm Nunclon surface dishes were purchased from Invitrogen/ThermoFisher (Carlsbad, CA, USA). A804598, BX430, ^{10}Panx inhibitory peptide, and Y-27632 were purchased from Tocris (Minneapolis, MN, USA). N-(p-amylcinnamoyl) Anthranilic Acid (ACA), Bromoenol lactone (BEL), SB-203580 (SB), PP2, IAA-94, and Ac-YVAD-CMK (YVAD) were purchased from Cayman Chemical (Ann Arbor, Michigan, USA).

Cell Culture

All human studies were reviewed and approved by the Institutional Review Board at Saint Louis University School of Medicine. Monocyte-derived macrophages were isolated as previously described with modifications (41). Blood obtained from healthy volunteers (12 males and 5 females, with some donors drawn more than once; aged 22–78) was centrifuged at 500 g for 10 min to isolate plasma, buffy coat layer, and erythrocytes. The buffy coat layer was removed, diluted 2:1 with cold, divalent-free physiological buffered saline (PBS), and then overlaid on 15 mL of Histopaque 1077 (Millipore Sigma, St. Louis, MO) in a 50 mL centrifuge tube. The tube was centrifuged at 900 g for 30 min with no brake to produce an interfacial layer of mononuclear cells and platelets. This layer was removed and then processed through three PBS wash and spin (250 g for 7 min) cycles. After the final spin, the pelleted cells were resuspended in 8 mL of a culture medium made of RPMI 1640, 7.5% heat-inactivated autologous plasma, 100U/L penicillin, 100 μg/mL streptomycin, and 1X Non-Essential Amino Acids (all from Life Technologies, Carlsbad, CA). For electrophysiology, monocytes were plated on 35 mm culture dishes. For dye uptake studies, monocytes were plated at 3.2×10^5 cells/mL on collagen-coated 13 mm glass coverslips (Gold Seal Cover Glass, Thermo Scientific, Waltham, MA) in 4-well plates (CELLTREAT Scientific Products, Pepperell, MA). For ELISA studies, cells were plated at 9.8×10^4 cells/well on clear-bottom 96-well plates. In all cases, cells were placed in a humidified 5% CO_2 incubator and left to rest for 2 hr after which the coverslips/plates were washed several times with warm PBS to remove non-adherent cells. The remaining adherent cells were cultured in culture medium (2 mL for dishes, 0.5 mL for 4-well plates, or 100 μL for 96-well plates) plus 10 ng/mL M-CSF (Millipore Sigma, St. Louis, MO) for 6–14 days. In some experiments, lipopolysaccharide (LPS, 10 μg/mL, Sigma-Aldrich Corp., St. Louis, MO) was added for 3 hr immediately preceding the start of the assays.

The mouse macrophage cell line J774A.1 (ATCC, Manassas, VA, USA) and HEK293 cells stably expressing human P2X7R were cultured in DMEM containing 10% FBS, 2 mM glutamine, 50 U/mL penicillin and 50 μg/mL streptomycin using standard protocols.

siRNA—30 nM each of three different Invitrogen Silencer Select Anoctamin 6 siRNAs (ID #s47040, #s225826, and #s225825) or 90 nM total negative control silencer select siRNA (#4390843) were transfected into human macrophages using 0.6% Invitrogen Lipofectamine RNAiMax in Invitrogen Opti-MEM Reduced Serum Medium (all products from ThermoFisher, Waltham, MA). Macrophages were studied 48 or 72 hr after transfection.

Reverse transcriptase PCR and real-time PCR—Total RNA was isolated from human macrophages using Invitrogen PureLink RNA Mini Kit (ThermoFisher, Waltham, MA). 2 μg of RNA was reverse transcribed in 20 μL for 1 h at 37 °C using the High-Capacity RNA-to-cDNA Kit (Applied Biosystems, Foster City, CA). Real-time PCR was performed in 20 μL of mixture (80 ng cDNA, 10 μL of 2 × SYBR Select master mix (Applied Biosystems #4472908), and 0.4 μM of each forward and reverse RT^2 qPCR primer assays (Ano6: #PPH19527A, β-actin (ACT): #PPH00073G, P2X1R:# PPH01871A, P2X4R: #PPH01349B, P2X7R:# PPH01489F) (Qiagen, Valencia, CA). Samples were analyzed in triplicate and target gene expression was normalized to ACT.

Patch Clamp Electrophysiology

Adherent macrophages were scraped from 35 mm plastic tissue culture dishes and then transferred to a recording chamber positioned on the stage of a Nikon inverted microscope continuously perfused with an extracellular solution (ECS) containing (in mM): 140 NaCl, 5.4 KCl, 0.2 $CaCl_2$, 10 glucose, and 10 HEPES at pH 7.4. Recordings began before the macrophages had a chance to attach to the glass bottom of the recording chamber; recordings from free-floating rounded macrophages increased the fidelity of the voltage-clamp and provided a platform for quick and efficient application of drugs. Whole-cell currents were recorded at room temperature with low resistance (2–4 MΩ), lightly fire-polished, borosilicate glass electrodes (1B150F, World Precision Instruments, Sarasota, FL) filled with a solution containing (in mM): 122 KCl, 32 KOH, 10 HEPES, and 10 EGTA at pH 7.4 and Axopatch 200B amplifiers (Molecular Devices, San Jose, CA). The holding potential was −60 mV unless otherwise indicated. Data were filtered at 5 kHz during acquisition and digitized at 10 kHz using an ITC-16 data acquisition board (Heka Electronics, Holliston, MA). Drugs were applied using triple-barreled theta glass and a Perfusion Fast-Step SF-77 System (Warner Instruments, Hamden, CT). Current-voltage curves were generated by measuring the currents resulting from 500 ms ramps of command voltage from −90 to 30 mV.

Pharmacology—Repetitive applications of ATP produce progressive facilitation of P2X7R-mediated currents (see Results). To quantify agonist potency, we measured peak agonist-gated current amplitudes for multiple concentrations of ATP from fully facilitated receptors, and then pooled the respective results for each concentration to yield a normalized current amplitude expressed as a fraction of the current caused by 2 mM ATP. These data were plotted as log (agonist concentration) versus normalized current using Prism 7

(GraphPad ,La Jolla, CA), and fit by nonlinear regression to calculate the concentration of agonist giving a half-maximal response (i.e., the EC_{50}).

Cell loading of AM esters—Macrophages plated on glass coverslips were incubated in ECS containing either BAPTA-AM (10 μM) in ECS with pluronic F-127 (0.1% final solution) for 60 min or calcein-AM (0.5 μM) for 30 min at 37ºC. The ester was removed by washing with ECS and the cells were used in downstream assays.

Dye Uptake—Macrophage permeabilization was assayed using the dyes YO-PRO-1 (5 μM), YOYO-1 (5 μM), carboxyfluorescein (0.5 mM), Lucifer yellow (0.5 mM), or calcein-AM (0.5 μM). Cells grown on coverslips were washed in ECS and then incubated with ATP (2 mM or 5 mM) or BzATP (300 μM) in ECS with and without the dyes for 15 min at 37°C. In some experiments, cells were pre-incubated for 30 min with the following compounds: A804598 (1 μM), BX430 (2 μM), tannic acid (20 μM), DIDS (100 μM), A01 (40 μM), NPPB (0.5 mM), ACA (50 μM), BEL (50 μM), carbenoxolone (20 μM), ^{10}Panx1 peptide (300 μM), colchicine (50 μM), IAA-94 (150 μM), Y-27632 (20 μM), SB-203580 (10 μM), PP2 (20 μM), or Ac-YVAD-CMK (100 μM). In Ca^{2+} free experiments, macrophages were pre-incubated with BAPTA-AM (10 μM) for 60 min followed by addition of YO-PRO-1 ± ATP (2 mM) in Ca^{2+} free ECS containing EDTA (1 mM). In experiments using ionophores, cells were incubated with YO-PRO-1 and nigericin (20 μM) or ionomycin (1 μM) for 30 min at 37°C. In experiments using Melittin (10 μM), cells were preincubated with ACA (50 μM) followed by 30 min incubation with YO-PRO-1, MEL, and ACA at 37°C. In the time-course experiments, YO-PRO-1 and calcein fluorescence were measured after ATP stimulation every 10 seconds for 15 min. The change in intracellular dye concentration was measured by fluorescence microscopy using an inverted epifluorescence microscope (Eclipse TE2000, Nikon) fitted with a CoolSnap CCD camera (Photometrics Scientific, Tucson, AZ) using 488/510 ex/em wavelengths. Molecular weights are expressed for the ionized forms of the dyes in solution.

Measurement of PLA2 activity—The activity of PLA2 was measured with a PLA2 assay kit (cat no. ab133090; Abcam, Cambridge, MA, USA). Macrophages were grown in 4-well dishes and stimulated with control ECS or 2 mM ATP ± ACA (50 μM) for 15 mins. Macrophages were then scraped and pelleted in microcentrigue tubes at 4,000 rpm for 5 mins. Cell pellets were then lysed in lysis buffer containing (in mM):150 NaCl, 25 HEPES, 5 EDTA, 1% Triton X-100, pH 7.4. Arachidonoyl thio-PC synthetic substrate was used to detect PLA2 activity. Hydrolysis of the arachidonoyl thioester bond releases a free thiol, which is detected by 5,5′-dithiobis-(2)-nitrobenzoic (DTNB) acid. Developed plates were read on a Biotek Neo Alpha Plate Reader plate reader with Gen5 software at 414 nm. (BioTek Instruments, Winooski, VT). Enzyme activity was normalized and expressed as a percentage of control macrophages.

Intracellular Cl^- Measurements—For measurement of intracellular chloride, macrophages were grown in 96-well plates at a density of 9.8×10^4 cells/well. Macrophages were stimulated in control ECS or with 2 mM ATP ± tannic acid (20 μM) or A01 (50 μM) for 15 mins. The supernatants were removed, deionized H_2O (200 μl per well) was added

and cells were scraped and placed into microcentrifuge tubes. The lysates were centrifuged at 10,000×*g* for 5 min. 100 μl supernatants were then transferred the to a new microcentrifuge tube and mixed with N-(Ethoxycarbonylmethyl)-6-methoxyquinolinium bromide (MQAE, 100 μM). The fluorescence (340 ex, 460 em) was measured by a Fluoroskan Ascent FL Microplate Fluorometer (Thermo Labsystems, San Diego, CA).

Cell Blebbing, Annexin V Binding, and Phagocytosis Assays—Human macrophages were incubated with or without ATP (2 mM) and antagonists in ECS for 15 min at 37°C, and then imaged on an inverted microscope. Cells were analyzed and quantified as the percentage of cells that displayed blebbing. For blebbing videos, 1 image was taken every 10 sec for 24 mins.

For Annexin V binding, macrophages were treated with ATP (2 mM) and antagonists for 5 min. After treatment, cells were incubated with Annexin V-FITC (BD Biosciences, San Jose, CA, USA) for 15 min at room temperature. Cells were subsequently analyzed using an inverted epifluorescence microscope. Annexin V was detected with 488/510 ex/em wavelengths and analyzed using ImageJ software.

For phagocytosis, macrophages plated in 35-mm dishes were scraped, pelleted at 4,000 rpm for 5 min, and resuspended with 40 μg/mL pHrodo Red *E. coli* BioParticles ± BzATP (300 μM) or ATP (2 mM) in ECS for 30 min at 37°C, followed by pelleting cells and resuspending with 15 μL fresh ECS. Cells were then added directly to a fluorescence microscope and pHrodo Red *E. coli* BioParticles were detected using 596/615 ex/em wavelengths.

Caspase-1 Assay—Macrophages grown on coverslips were treated with or without LPS (10 μg/mL) in ECS for 3 hrs. The cells were then preincubated with A804598 (1 μM), tannic acid (20 μM), A01 (40 μM), Ac-YVAD-CMK (100 μM), MCC950 (10 μM), or IAA-94 (150 μM) in ECS for 30 min. Cells were then treated with or without BzATP (300 μM) ± antagonists for 30 min. The cells were incubated with 1 × FAM-YVAD-FMK (caspase-1 FLICA; Immunochemistry Technologies, Bloomington, MN, USA) at 37°C for 90 min, with gentle mixing every 20 min. The cells were washed 3X with Apoptosis Wash Buffer (Immunochemistry Technologies), and placed in fresh ECS. Coverslips were then added directly to an epifluorescence microscope and caspase-1 FLICA was detected using 488/510 ex/em wavelengths.

ROS Assay—Human macrophages grown on coverslips were primed with or without LPS (10 μg/mL) for 3 hrs or 40 μg/mL pHrodo Red *E. coli* BioParticles for 1 hr followed by loading cells with 0.1X DCFH-DA (Cell Biolabs, San Diego, CA) in ECS for 30 min at 37°C. J774A.1 mouse macrophages were grown on coverslips overnight and loaded with DCFH-DA. Coverslips were then added directly to an epifluorescence microscope and imaged after ATP stimulation every 10 secs for 30 min using 488/510 ex/em wavelengths.

ELISA

Macrophages seeded in 96-well plates at a concentration of 9.8×10^4 cells/well were primed with or without 10 μg/ml LPS for 3 hrs in ECS followed by preincubation with A804598 (1

μM), tannic acid (20 μM), or A01 (40 μM) for 30 min, and subsequently stimulated with BzATP (300 μM) ± antagonists for 30 min at 37°C. Supernatants were collected and kept frozen at −20°C until analysis. IL-1β was evaluated with ELISA using the Invitrogen IL-1 beta Human Uncoated ELISA Kit (Cat # 88–7261-88) according to the manufacturer's protocol. Developed plates were read on a Biotek Neo Alpha Plate Reader plate reader with Gen5 software. (BioTek Instruments, Winooski, VT).

LDH Release Assay—Macrophages seeded in 96-well plates at a concentration of 9.8×10^4 cells/well were primed with or without LPS (10 μg/mL) for 3 hrs, followed by incubation with A804598 (1 μM) or tannic acid (20 μM) for 30 min, and subsequently stimulated with BzATP (300 μM) or ATP (2 mM) ± A804598 or tannic acid for 30 min at 37°C. Untreated cells served as the negative control while lysed cells served as the positive control. 50 μL of cell supernatant was collected and used to detect LDH activity with the CytoTox96 Non-Radioactive Cytotoxicity Kit (Promega, Madison, WI, USA) according to the manufacturer's instructions.

Imaging Analysis—In all fluorescence microscopy observations, a field of 10–50 cells was photographed using bright field illumination to get an image of cell morphology. Then, fluorescence microscopy and dyes were used to image specific functional properties. We used μManager 1.4 (42) and Fiji (43) to acquire data and perform analysis. Exposure, binning, and frame rate varied with experiment.

Corrected total cell fluorescence (CTCF) in relative fluorescence units (RFU) was measure as:

CTCF = whole cell signal - (area * background signal)

where "whole cell signal" equals the sum of the intensity of the pixels for one cell; "area" equals the number of pixels defining the cell; and "background signal" equals the average signal per pixel for a region devoid of cells but close to the cell of interest (36).

Statistical Analysis

Data were analyzed using GraphPad Prism, and reported as mean ± s.e.m. Student's t-test (for paired or unpaired samples as appropriate), and analysis of variance with Tukey post-test were used for statistical analysis. $p < 0.05$ was accepted as a significant difference.

Results

Human macrophages express multiple P2X receptors

We used RT-qPCR to measure mRNA expression for P2XRs in monocyte-derived human macrophages after seven days in culture. Strong expression was observed for P2X1R, P2X4R and P2X7R obtained from three different donors (Fig. 1a). This finding is in accordance with previous studies reporting functional evidence for these receptors in monocyte-derived human macrophages (44–48).

ATP evokes biphasic membrane currents in human macrophages

We used patch-clamp electrophysiology to measure the ATP-gated membrane currents of human macrophages. An initial short (3 s) pulse of ATP (2 mM) produced a biphasic current composed of a desensitizing initial component followed by a sustained plateau (Fig. 1b), indicating the involvement of more than one P2XR subtype. Subsequent ATP applications applied every 15 s evoked only the sustained current, as expected if the short-lived early component was caused by desensitizing P2X1Rs and/or P2X4Rs (49). To test this hypothesis, we used a concentration of ATP (100 μM) that is below the threshold for activation of the human P2X7R, which likely comprises the sustained current (48, 50, 51). Stimulation of macrophages with 100 μM ATP activated only the desensitizing current which showed a progressive reduction in peak current amplitude with repetitive applications spaced 15 s apart, and recovered to full amplitude following a 3 min wait (Supplemental Fig 1a-e). Moreover, application of the synthetic agonist, BzATP (10 μM), triggered desensitizing currents (peak current equals 10.1 ± 3.3 pA/pF, n = 4), whereas lower concentrations (100 nM) of BzATP produced no measurable current. Since P2X1Rs are maximally activated by 100 nM BzATP (52), our data suggest that P2X4Rs are responsible for the desensitizing current, a finding in keeping with a recent report of P2X4R-mediated changes in intracellular Ca^{2+} concentrations in human macrophages (48). Because all of the protocols described in this paper use either repeated or sustained applications of agonists that render P2X1Rs and P2X4Rs inactive, our experiments going forward only consider the functional contribution from non-desensitizing P2XRs.

The sustained current facilitates as expected for human P2X7Rs

Repetitive 3 s applications of the higher concentration of ATP (2 mM) lead to a progressive growth of the sustained current by 1857% ± 558% in 15 min (n = 31; Fig 1c), a hallmark property of P2X7R activation known as “facilitation” (33, 53, 54). The reversal potential of the fully facilitated current was −1.4 ± 0.3 mV (n = 29) as expected for a non-selective cation current through a P2XR (Fig. 1d,e). We calculated the EC_{50} of ATP after full facilitation by plotting peak current amplitude against agonist concentration. We found that the amplitude of the facilitated current increased as a function of ATP concentration with an EC_{50} of 2 mM (Fig. 1f). After facilitation, 100 μM ATP, a concentration which maximally activates desensitizing human P2X1Rs and P2X4Rs (52), failed to generate inward currents, confirming our assumption that the P2X7R is the only remaining receptor capable of generating the sustained responses we see using the protocols described here. Repetitive applications of the more potent P2X7R agonist, BzATP (300 μM), also evoked facilitating nonselective cation currents (Supplemental Fig 1f-i). Furthermore, preincubation with the selective non-competitive P2X7R antagonist A804598 (1 μM) resulted in robust reduction (91.5 ± 0.8%, n=9) of the peak current amplitude of the ATP-gated current (Fig. 1g,h). Taken together, our data support recent reports of desensitizing P2XRs in human macrophages and provide direct evidence that these same cells express facilitating P2X7Rs (46, 49).

P2X7Rs induce cation-selective dye uptake in macrophages

In addition to stimulating ion channel activity, P2X7Rs also permeabilize cell membranes to polyatomic molecules, a process associated with the release of IL-1β, interferon-γ, and ROS/NO in murine macrophages (39, 55). The cationic nucleic acid binding dye YO-PRO-1 is a commonly used fluorescent reporter of membrane permeabilization (56). Therefore, to more closely examine the signaling pathway(s) underlying permeabilization of human macrophage P2X7Rs, we characterized the uptake of YO-PRO-1 (376 Da, 5 μM). We found that human macrophages are impermeable to YO-PRO-1 in the absence of extracellular ATP. However, in keeping with published reports (45, 57), we saw significant uptake of YO-PRO-1 during 15 min applications of either ATP (2 mM) or BzATP (300 μM) (Fig. 2a). We characterized the pharmacology of YO-PRO-1 uptake using subtype selective P2XR antagonists. Permeabilization was completely blocked by the P2X7R antagonist A804598 (1 μM) but unaffected by the P2X4R antagonist BX430 (2 μM), indicating that P2X7Rs but not P2X4Rs are essential for dye uptake (Fig 2b,c). Importantly, dye uptake was not an artifact of cell lysis as a 30 min stimulation with 2 mM ATP or 300 μM BzATP did not evoke release of lactate dehydrogenase, a marker of cell viability (Fig. 2d). Moreover, prolonged stimulation of human macrophages with ATP or BzATP did not impact their ability to phagocytose *E. coli* particles (Fig 2e,f), providing additional evidence that the cells are viable and capable of functioning as expected.

Murine macrophages utilize separate pathways for ATP-gated uptake of anionic and cationic dyes (58). To better understand the permeabilization pathway in human macrophages, we measured uptake of the anionic dyes Lucifer yellow (443 Da, 0.5 mM) and carboxyfluorescein (376 Da, 0.5 mM). Surprisingly, neither of these anionic dyes crossed the surface membrane of human macrophages during a 15 min stimulation with 2 mM ATP (Fig. 3a,b). Furthermore, P2X7R activation was unable to drive anion efflux from macrophages pre-loaded with anionic calcein (622 Da, 0.5 μM) (Fig. 3c,d).

Anionic Lucifer yellow and calcein have larger molecular weights than cationic YO-PRO-1, and the inability of the anionic dyes may simply reflect their large size. To firmly rule out size as a limiting factor for the passage of anionic dyes, we measured uptake of the cationic dye, YOYO-1 (750 Da, 5 μM), whose molecular weight far exceeds that of the anions. We found that 2 mM ATP stimulated YOYO-1 uptake (Fig. 3e,f), proving that size is not responsible for the difference in the magnitude of ATP-evoked diffusion of anions and cations into human macrophages. Further, because cytolytic pathways are non-selective by nature, the ability of human macrophages to discriminate between cationic and anionic dyes provides additional evidence that permeabilization is a noncytolytic process in human macrophages.

Permeabilization of human monocyte-derived macrophages is independent of Pannexin-1

While some studies suggest that cationic dyes pass directly through the P2X7R ion channel, others point to the involvement of additional pathways (24, 32, 45, 59–62). One such route is the hemichannel pannexin-1, reported to mediate human alveolar and THP-1 macrophage dye uptake and IL-1β release downstream of the P2X7R (35). Based on these findings, we decided to measure the impact of two pannexin-1 blockers (20 μM carbenoxolone, CBX;

and 300 μM ^{10}panx1 peptide) on dye uptake in monocyte-derived human macrophages. We preincubated the cells in CBX or ^{10}panx1 for 30 min and then measured YO-PRO-1 uptake in the presence of 2 mM ATP. Neither antagonist prevented dye uptake (Fig. 4a,b). Our negative results conflict with those obtained using human lung alveolar macrophages where uptake of ethidium is significantly reduced in the presence of ^{10}panx1 (35), suggesting that tissue specific paracrine signaling may recruit distinct permeabilization pathways in resident macrophages.

We also studied the role of K^+ efflux since it activates pannexin-1 channels in murine macrophages (63, 64). We applied nigericin (20 μM), a K^+/H^+ ionophore, to human macrophages and found that it does not stimulate YO-PRO-1 uptake (Fig. 4a,b). Moreover, we substituted equimolar K^+ for extracellular Na^+ to reduce the chemical driving force for K^+ across the surface membrane and we were still able to trigger YO-PRO-1 uptake with 2 mM ATP (Fig 4b). Taken together, our results suggest that pannexin-1 channels and K^+ efflux do not contribute to permeabilization of monocyte-derived human macrophages.

Colchicine does not impact cationic dye uptake

Disruption of microtubules with colchicine blocks ATP-evoked uptake of YO-PRO-1, ROS generation, and IL-1β release in mouse macrophages (39). To determine if the same holds true in humans, we incubated cells with colchicine (50 μM) for 30 min. We measured no impact of colchicine on ATP-induced YO-PRO-1 uptake (Fig. 4b). Importantly, these results indicate that P2X7R-induced permeabilization exhibits unique requirements between primary murine and human macrophages.

P2X7R-evoked dye uptake is inhibited by Cl^- channel blockers

Primary mouse macrophages and human THP-1 cells express Anoctamin 6 (Ano6; *a.k.a.*TMEM16F), a Ca^{2+}-activated Cl^- channel linked to a number of innate immune responses downstream of the P2X7R (65, 66). To determine if a Cl^- channel participates in P2X7R-mediated dye uptake by human macrophages, we pre-incubated cells in one of a range of Cl^- channel blockers, and then measured the ability of 2 mM ATP to stimulate YO-PRO-1 uptake. All four blockers (tannic acid (TA), DIDS, NPPB, and A01) significantly inhibited YO-PRO-1 uptake (Fig. 5a,b), suggesting a role for a Cl^- channel in the action of ATP. To provide further support, we used a fluorescent measure of intracellular Cl^- concentration to assay changes in the intracellular milieu. Human macrophages were stimulated with ATP (2 mM) for 15 mins followed by removal of cell supernatants and lysis of cells with pure deionized H_2O. Addition of MQAE to the cell lysates revealed a significant decrease in fluorescence upon ATP stimulation, suggesting the action of an inward flux of Cl^- in response to application of extracellular ATP. Importantly, tannic acid and A01 significantly reduced ATP-induced Cl^- influx (Fig. 5c). Thus, the pathway between the P2X7R and the ultimate effector of membrane permeabilization includes an undefined but essential Cl^- channel.

Permeabilization is not dependent on a change in $[Ca^{2+}]_i$

Next, we tested the dependence of dye uptake on $[Ca^{2+}]_i$ to address the controversy regarding the role of this divalent cation in permeabilization (38, 67) and to determine if

Ca^{2+} flux was responsible for downstream Cl^- channel activation. We incubated human macrophages in 10 μM BAPTA-AM for 60 min at room temperature to chelate intracellular Ca^{2+} and then applied ATP and YO-PRO-1 dye in the presence of a Ca^{2+}-free ECS containing 1 mM EDTA. We saw no difference in the magnitude of YO-PRO-1 uptake by comparison to experiments executed in the absence of Ca^{2+} chelation (red bar of Fig. 5b). Furthermore, direct stimulation of Ca^{2+} influx with ionomycin (1 μM) did not cause YO-PRO-1 uptake (Fig. 5d,e). Thus, we find that ATP-mediated dye uptake in human macrophages is not dependent on a change in $[Ca^{2+}]_i$ and provide evidence against activation of the Cl^- channel by a P2X7R-mediated Ca^{2+} flux.

Interestingly, higher levels of extracellular Ca^{2+} (2 mM) robustly inhibited YO-PRO-1 uptake (green bar of Fig. 5b). To explain this observation, we measured ATP-induced (2 mM) inward currents in the presence of high extracellular Ca^{2+} (2 mM) and found that it first facilitates to a new peak that subsequently declines with continued repetitive stimulation (Supplemental Fig. 2a,b). As a consequence of run-down, the inward current density is reduced by high extracellular Ca^{2+} (25.6 vs. 42.6 pA/pF, Supplemental Fig. 2c). However, a decrease in the current density alone cannot explain the prevention of dye uptake as stimulating macrophages with a lower concentration of ATP (500 μM) resulted in currents that were smaller (15 pA/pF) on average than that we typically measured after rundown, but still capable of triggering significant cell permeabilization (Supplemental Fig. 2c-e). Previous reports attributed current run-down to recruitment of Receptor Protein Tyrosine Phospatase-β which dephosphorylates a key residue in the channel of the P2X7R (68). Thus, high extracellular Ca^{2+} may prevent macrophage permeabilization via recruitment of a phosphatase, a hypothesis worth pursuing in the future.

The P2X7R activates PLA_2–stimulated dye uptake independently of tyrosine kinases

Previous studies in primary mouse macrophages found that P2X7Rs activate dye uptake independently of Ca^{2+} flux by activation of the phospholipid hydrolyzing enzyme phospholipase A2 (PLA_2) (69). Therefore, we studied the PLA_2 dependence of permeabilization by preincubating human macrophages with the broad spectrum PLA_2 inhibitor, ACA (50 μM), and found a nearly complete inhibition of ATP-induced YO-PRO-1 dye uptake (Fig. 6a,b). This suggests that the P2X7R stimulates downstream Cl^- channels by activating calcium-independent PLA_2. To further support this hypothesis, we found that the PLA_2 activator Melittin (10 μM) induced YO-PRO-1 uptake, which was completely blocked by ACA (50 μM) (Fig. 6c,d). It is important to note that the PLA_2 inhibitor, BEL, was previously reported to inhibit ATP-induced murine macrophage inflammation in a PLA_2 independent manner (70). Instead, BEL targeted serine proteases that are critical for inflammasome activation. Thus, as a control for these pharmacological inhibitors, we next measured PLA_2 activity directly with a colorimetric assay that detects PLA_2-mediated hydrolysis of the synthetic substrate arachidonoyl thio-PC. We found that macrophages treated with 2 mM ATP for 15 mins displayed robust activation of PLA_2, and this activity was significantly reduced by pretreatment with ACA (50 μM) (Fig. 6e).

We also tested the effect of inhibiting p38 MAPK/Src tyrosine kinases on ATP-induced YO-PRO-1 uptake because ATP-dependent stimulation of phospholipase activation is reported to

occur downstream of these kinases (71–73). However, neither the selective p38 MAPK inhibitor, SB-203580 (10 μM), or the selective src tyrosinse kinase inhibitor, PP2 (20 μM), prevented YO-PRO-1 uptake (Fig. 6f,g). Therefore, our data indicate that P2X7R-mediated PLA_2 and Cl^- channel activation occurs independently of p38 MAPK or src tyrosine kinase stimulation.

Facilitation of P2X7Rs is prevented by inhibition of PLA_2 and Cl^- channels

We found that long or repeated applications of ATP facilitate currents (see Fig 1c) and permeabilize membranes (see Fig 2b) in primary human macrophages, two temporally related processes (33). Since membrane permeabilization is prevented by preincubation with Cl^- channel blockers (see Fig 5b), we next investigated the ability of these drugs to block facilitation. We found that tannic acid (20 μM; Fig 7a-d) and A01 (40 μM; Fig 7e,f) significantly inhibited the facilitated currents of human macrophages. While the inhibition by A01 was fully reversible (Fig. 7f), the inhibition by tannic acid was not (Fig. 7b,d). Reapplying tannic acid did not block the current that remained after the first application of tannic acid (Fig. 7b). In addition, exposing macrophages to tannic acid before facilitation occurred prevented current growth (Fig. 7c,d). We hypothesize that current facilitation depends on P2X7R-mediated recruitment of Cl^- channels that are sensitive to tannic acid and A01.

If P2X7Rs stimulate Cl^- channels through a PLA_2-dependent pathway, then the PLA_2 antagonist should block facilitation of ATP-gated currents. We found that 50 μM ACA reversibly blocked a substantial portion of the facilitated current (Fig. 7g,h). Thus, our data suggest that the P2X7R activates PLA_2, which is required for both Cl^- channel-dependent ionic current facilitation and membrane permeabilization.

P2X7R-induced macrophage blebbing requires Cl^- channels

Prolonged activation of P2X7Rs induces significant membrane blebbing (74), an essential process that enhances survival of injured cells (75). We found that membrane permeabilization of human macrophages by ATP is unaffected by colchicine, a drug that disrupts microtubules (see Fig 4). This was surprising because several lines of evidence suggest that P2X7Rs can dramatically influence macrophage function by interacting with the cytoskeleton. Specifically, P2X7R-induced activation of p38 MAPK and Rho drives actin reorganization and coincident membrane blebbing in murine macrophages via mechanisms distinct from IL-1β release (23, 30, 76). To determine if P2X7Rs evoke membrane blebbing in human macrophages, we applied 2 mM ATP for 15 min while monitoring cell morphology. We found that ATP caused extensive membrane blebbing (Supplemental Video 1), which was completely blocked by the P2X7R antagonist A804598 (1 μM) but not the P2X4R antagonist BX430 (2 μM) (Fig. 8a,b). Moreover, the process is reversible as a 30 min washout of ATP resulted in retraction of membrane blebs (Fig. 8b, Supplemental Video 2). In accordance with our permeabilization data, we found that pannexin-1 blockers, p38 MAPK/src tyrosine kinase antagonists, and colchicine had no effect on the ability of ATP to induce bleb formation (Fig. 8c). Importantly, the Cl^- channel inhibitors tannic acid, DIDS, AO1, and NPPB caused nearly a complete block of P2X7R-dependent membrane blebbing (Fig. 8d). Interestingly, chelation of intracellular and extracellular Ca^{2+} with BAPTA and

EDTA significantly inhibited ATP-induced bleb formation (Fig. 8d), suggesting that Ca^{2+} plays a critical role in cytoskeletal rearrangement (54). The fact that removing Ca^{2+} blocks bleb formation but has no effect on membrane permeabilization also suggests that these two functions result from divergent signaling pathways. However, direct stimulation of Ca^{2+} influx with ionomycin (1 μM) was unable to stimulate blebbing (Fig. 8d), suggesting that this process requires the P2X7R to drive more than solely Ca^{2+} flux. Moreover, higher levels of extracellular Ca^{2+} blocked ATP-induced membrane blebbing in macrophages, but not in HEK293 cells stably expressing human P2X7Rs (Supplemental Fig. 2f). These results suggest that the pathway leading to current run-down in human macrophages under these conditions also acts to prevent Cl^- channel mediated blebbing.

As P2X7 dependent K^+ efflux was recently shown to directly promote Ca^{2+} influx and inflammatory responses in mouse macrophages (34), we next tested the dependence of blebbing on K^+ efflux. Prevention of K^+ efflux by the addition of high KCl (130 mM) to the extracellular solution robustly prevented ATP-induced membrane blebbing (Fig. 8d). However, direct stimulation of K^+ efflux with Nigericin was unable to promote blebbing. These findings indicate that both P2X7R driven K^+ efflux and Ca^{2+} influx are required for bleb formation.

Membrane blebbing proceeds through a PLA_2- and ROCK-dependent pathway

PLA_2 is part of the signaling pathway that links the P2X7R to membrane permeabilization (see Fig 6). Inhibition of PLA_2 suppresses P2X7R-mediated membrane blebbing in murine osteoblasts (77). Does PLA_2 play a role in membrane blebbing in human macrophages? To answer this question, we applied ACA and BEL to inhibit PLA_2 and saw a near complete block of bleb formation (Fig. 8d). Furthermore, in agreement with previous studies that found PLA_2 activates P2X7R-induced blebbing via activation of the Rho-associated, coiled-coil containing protein kinase (ROCK) in murine cells (23, 77), we observed that the selective ROCK inhibitor Y-27632 (20 μM) completely prevented membrane blebbing in human macrophages (Fig. 8d).

Taken together, our results provide evidence that P2X7R activation of PLA_2 is required for human macrophage blebbing and this process depends on ROCK-mediated cytoskeletal rearrangement. Our finding that the ability of ATP to induce blebbing is inhibited by Cl^- channel blockers suggests that these channels play a key role in the initiation and/or maintenance of this response.

Cl^- channels drive phosphatidylserine exposure downstream of the P2X7R

Phosphatidylserine (PS) exposed on the outer leaflet of the plasma membrane serves as an “eat me” signal for phagocytosis of dying cells (28, 29). High concentrations of ATP stimulate rapid PS exposure in murine cells by activating P2X7Rs (25–27). We found that 2 mM ATP rapidly induced PS translocation in human macrophages as measured by an annexin V binding assay (Fig. 8e,f). Translocation was robustly inhibited by both P2X7R (A804598) and Cl^- channel (tannic acid and A01) antagonists (Fig. 8e,f). The PS switch did not depend on a rise in $[Ca^{2+}]$ as BAPTA-loaded macrophages stimulated in ECS containing EDTA maintained their ATP-induced PS flip (Fig. 8e,f). Moreover, Y-27632 did not prevent

PS translocation (Fig. 8f), which suggests that ROCK-dependent macrophage blebbing and ROCK-independent PS flip have distinct requirements. Together, these results suggest that that a Ca^{2+}-independent Cl^- channel is responsible for PS exposure downstream of P2X7R activation.

Cl^- channel antagonists block P2X7R-mediated caspase-1 activation and IL-1β release

We next investigated the contribution of Cl^- channels to P2X7R-dependent caspase-1 activation. Caspase-1 processes pro-IL-1β and pro-IL-18 to mature proinflammatory cytokines (78) and cleaves Gasdermin D to release its pyroptotic pore-forming N-terminus (79). Activation of caspase-1 is a hallmark property of P2X7Rs in many tissues including murine macrophages (80), and we were interested to see if caspase-1 activation is sensitive to Cl^- channel blockers in human macrophages. We measured activated caspase-1 enzyme using a fluorescence assay, and found that 300 μM BzATP caused significant activation in both resting and LPS-primed macrophages (Fig. 9a,b). To confirm the enzymatic selectivity of the dye, treatment of macrophages with the irreversible caspase-1 inhibitor, Ac-YVAD-CMK (100 μM), blocked BzATP-induced caspase-1 staining (Fig. 9b). Caspase-1 activation was dependent on P2X7Rs as it was blocked by A804598 (Fig. 9a,b). Moreover, P2X7R-driven caspase-1 activation required NLRP3 inflammasome activation, as the selective NLRP3 inhibitor, MCC950, significantly reduced caspase-1 activation (Fig. 9b). In accordance with our studies on membrane blebbing, permeabilization, and PS translocation, the ATP-dependent activation of caspase-1 was inhibited by Cl^- channel blockers in both LPS treated and untreated macrophages (Fig. 9a,b).

To further investigate the mechanism of caspase-1 activation, we measured the ability of the P2X7R to stimulate macrophage production of reactive oxygen species (ROS), which was previously reported to trigger inflammasome assembly in mice (34). We loaded cells with DCFH-DA, a molecular probe that forms fluorescent dichlorofluorescein upon oxidation, thus providing a readout of ROS production. To validate the assay, we measured ROS production in immortal mouse J774A.1 macrophages and measured rapid ROS production upon ATP stimulation (green bars, Fig. 9c). Further, application of 1 mM H_2O_2 to human macrophages caused a measurable increase in fluorescence (red bar, Fig. 9c). In stark contrast, ATP stimulation of human macrophages primed with LPS or *E. coli* particles did not cause ROS production (Fig. 9c). Thus, our data show that ATP-evoked activation of caspase-1 does not proceed through a ROS-dependent pathway in human macrophages, and suggest distinct caspase-1 activation mechanisms exist between rodent and human macrophages.

Since caspase-1 is also responsible for Gasdermin D induced large membrane-pore formation, we investigated whether caspase-1 activated pores are required for P2X7R-dependent permeabilization and blebbing in unprimed macrophages. Treatment of human macrophages with the caspase-1 inhibitor, Ac-YVAD-CMK (100 μM), did not prevent ATP-induced YO-PRO-1 uptake or blebbing (Fig. 9d-f). Therefore, our data indicates that while P2X7Rs do stimulate caspase-1 activation, this process is not essential for dye uptake and cytoskeletal rearrangement in the absence of LPS.

P2X7R-dependent activation of caspase-1 is a potent stimulus for IL-1β processing and release (81). Therefore, we studied the contribution of Cl^- channels to P2X7R induced IL-1β release. We were unable to detect IL-1β in either the lysate or supernatant from un-primed macrophages stimulated with BzATP in the absence of LPS (Fig. 9g). Thus, inflammasome assembly does not rely on LPS, as BzATP induced caspase-1 activation occurred in the absence of stimulation (see Fig. 9b). In contrast, transcription of pro-IL-1β required LPS treatment. Application of BzATP to LPS primed macrophages resulted in significant IL-1β release, a process inhibited by the P2X7R antagonist, A804598 (Fig. 9g). Notably, both A01 and tannic acid inhibited BzATP-induced IL-1β release (Fig 9g), suggesting a role for Cl^- channels in P2X7R-dependent cytokine release. Furthermore, BzATP also caused significant cytotoxicity of LPS-primed macrophages as measured by LDH release, which was prevented by both A804598 and tannic acid (Fig. 9h). Our findings show that IL-1β release and inflammasome-mediated cell death follow P2X7R activation and occur downstream of Cl^- channel activation.

P2X7R functions independently of Ano6 and CLICs in human macrophages

A major finding of the work described here is that Cl^- channel blockers prevent P2X7R-induced innate immune functions of human macrophages including membrane permeabilization, blebbing, current facilitation, phospholipid scrambling, caspase activation, and IL-1β release. The molecular identity of the Cl^- channel responsible for these processes is unknown. In an attempt to uncover the identity, we performed studies of two putative Cl^- channels, Ano6 and Cl^- intracellular channels (CLICs), which are implicated in innate immune functions of murine macrophages.

Ano6 is a Ca^{2+} and PLA_2-activated Cl^- channel and an essential component of innate immunity (65, 82). We significantly reduced Ano6 gene expression by 76.7% in human macrophages using three different siRNAs (Supplemental Fig 3a). Despite this fact, we found that neither the ATP-gated current density nor facilitation were significantly affected 72 hr after silencing Ano6 (Supplemental Fig 3b-d). Moreover, YO-PRO-1 uptake, membrane blebbing, PS switch, and IL-1β release were unaffected by Ano6 knockdown (Supplemental Fig 3e-h). Thus, it seems unlikely that the effects we see with Cl^- channels blockers reflect an inhibition of Ano6 channels in human macrophages.

CLICs are soluble and membrane-associated proteins whose biological functions are poorly understood (83). A recent report suggests that extracellular ATP activates CLICs-dependent NLRP3 inflammasome activation in mouse macrophages (84). We tested for P2X7R-mediated activation of CLICs in human macrophages using the inhibitor IAA-94 (150 μM). Supplemental Fig. 4 shows that neither dye uptake, blebbing, PS flip, nor caspase-1 activation are inhibited by IAA-94. Therefore, CLICs are not required for these functions downstream of P2X7R activation in human macrophages.

Discussion

Our present results indicate that the P2X7R requires activation of a downstream Cl^- channel for stimulation of several innate immune functions in monocyte-derived human macrophages. Upon stimulation with extracellular ATP, an immediate whole-cell current is

activated that initially desensitizes and subsequently facilitates upon prolonged channel activation. Our results are in accordance with previous studies showing that human macrophages contain desensitizing P2XR1s (44) and P2X4Rs (48) as well as facilitating P2X7Rs (45, 46). Importantly, our study only considers the functional contribution from non-desensitizing P2X7Rs, as we mimic conditions of chronic inflammation and cellular injury by using sustained applications of ATP that prevent reactivation of desensitizing receptors. Our results show that P2X7Rs enable permeation of large polyatomic cations across the plasma membrane while excluding anions. We propose a model in which the P2X7R stimulates PLA_2-dependent activation of a Cl^- channel, which functions to activate or modulate macrophage permeabilization, blebbing, phosphatidylserine translocation, caspase-1 activation, and IL-1β release (Fig. 10).

Our data shows that stimulation of P2X7Rs with ATP or BzATP robustly permeabilizes human macrophages as measured by the uptake of the polyatomic cationic dye YO-PRO-1. Despite the considerable effort of numerous laboratories, the precise pathway underlying dye uptake is largely unresolved (32). Tissue specific variability may partially explain the lack of a unifying hypothesis. For example, the ATP-release channel, pannexin-1, is reported to transduce YO-PRO-1 uptake in resident human alveolar macrophages obtained from lung lavage (35). In stark contrast, we find no effect of pharmacological inhibition of pannexin-1 on the YO-PRO-1 uptake of monocyte-derived human macrophages. The fact that pannexin-1 regulates dye uptake in one but not the other type of human macrophage suggests that tissue-specific signals might serve as paracrine regulators of membrane permeabilization. This should not be surprising considering the heterogeneity of macrophages under physiological conditions (85), although it was not previously demonstrated for P2X7Rs, pannexins, and subtypes of human macrophages. Species-dependent differences are also apparent. For example, murine (58) but not human (see Fig 3) macrophages readily pass anionic dyes, and colchicine blocks YO-PRO-1 uptake in mouse (39) but not human (see Fig 5) macrophages. Additionally, the activation state of the macrophage may play a permissive role. For example, Marques-da-Silva *et al* established that infecting resident murine macrophages with the parasite *Leishmania amazonensis* changed the character of ATP-induced membrane permeabilization (86). Specifically, they found that uptake of anionic dye was up-regulated after infection whereas the passage of cationic dyes was robustly reduced (87). These suggest that murine macrophages can regulate the ATP-dependent passage of charged molecules across their surface membranes in response to external stimuli. Our study utilized human monocyte-derived macrophages differentiated in the presence of M-CSF, a growth factor that polarizes macrophages toward the anti-inflammatory M2 state (88) and may therefore influence the macrophage permeabilization pathways. These and other differences highlight the need for more extensive studies of primary human tissues, which represent the best models of human disease.

In agreement with previous reports in murine macrophages and human THP-1 cells (65), we find that uptake of YO-PRO-1 by human macrophages is blocked by several nonselective Cl^- channel antagonists (tannic acid, A01, DIDS, and NPPB). Because we also measured an ATP-gated influx of Cl^-, we conclude that uptake of dyes by human macrophages requires activation of a Cl^- channel. The exact role and identity of the Cl^- channel are still unknown.

It is possible that it functions as a transmembrane pathway for dye entry, although the biophysics that explain how cationic dyes permeate anion channels is difficult to understand. Some Cl^- channels show considerable cation permeability and form pores large enough to pass YO-PRO-1; members of the anoctamin family come to mind in this respect (89–91). Thus, it is possible that cationic dyes cross the membrane through such a non-selective "Cl^-" channel, although our finding that that cationic but not anionic dyes permeate human macrophages (see Fig. 3) would seem to rule this out. The more plausible hypothesis is that the P2X7R forms the dye-permeable pathway, and in fact, there is convincing evidence demonstrating direct permeation of cationic dyes through the P2X7R pore (60). However, at present, we have no data that conclusively identify the permeation pathway, which is why we show it as a separate channel in the cartoon of Figure 10.

We found that ATP-gated dye-uptake is inhibited by PLA_2 antagonists, suggesting that the P2X7R activity is sensitive to the lipid environment surrounding the channel. In a recent report, Karasawa *et al.* measured the effect of membrane lipids on reconstituted P2X7R channels and found direct effects of phosphatidylglycerol, sphingomyelin, and cholesterol on YO-PRO1 uptake (61). Thus, our finding that ATP-dependent permeabilization of human macrophages requires PLA_2 activation suggests the possibility that this enzyme facilitates pore opening by releasing membrane phospholipids which feeds back on P2X7R channel activity. In fact, we find that PLA2 antagonists indeed alter P2X7R current facilitation. However, it is also possible that PLA_2 indirectly triggers P2X7R-mediated dye uptake through an action on an upstream Cl^- channel. This could occur as the result of a change in anion concentration across the membrane in a manner reminiscent of the effect of K^+ efflux on NLRP3 inflammasome activation (92), or through a protein-protein interaction with a component of the regulatory pathway.

We considered the possibility that Ano6 may be the Cl^- channel responsible for innate immunity downstream of P2X7Rs. We investigated Ano6 because it acts as an ATP-sensitive phospholipid scramblase and ion channel in murine macrophages (65, 93, 94) and could thus explain the effects we see in human macrophages. In murine cells, Ano6 is activated by inflammatory mediators that increase $[Ca^{2+}]_i$, produce ROS, activate Fas ligand (FasL), or stimulate PLA_2 (95, 96). In human macrophages, we found that permeabilization was not impacted by chelation of Ca^{2+} but was inhibited by preventing activation of PLA_2. However, selective silencing of the Ano6 gene was unable to block P2X7R mediated permeailization. Therefore, at present, the molecular identity of the Ca^{2+}-independent Cl^- channel involved in the regulation of the ATP-evoked response remains unknown. Positive identification requires a complete genomic and electrophysiological charaterization of human macrophages, studies that should ultimately uncover the channels or transporters directly responsible for dye uptake into cells. Such work is beyond the scope of the present investigation but future experiments designed to explore this should be pursued.

In addition to permeabilization, P2X7Rs are also potent stimulators of several innate immune functions. Notably, these channels trigger actin reorganization and subsequent membrane blebbing, which is linked to stimulation of p38 MAPK and Rho-associated kinase (23, 77). Here we report that ATP evokes membrane blebbing of human macrophages in a manner that depends on K^+ efflux, a rise in $[Ca^{2+}]_i$, and activation of PLA_2, ROCK, and Cl^-

channels. The differential K^+ and Ca^{2+} flux requirements of membrane blebbing and permeabilization indicates that these two events are ultimately executed through separate pathways. Our results using Y-27632, a selective inhibitor of ROCK, agree with previous findings in mouse osteoblasts which established that membrane blebbing stems from PLA_2 mediated release of lysophosphatidic acid that in turn activates Rho-dependent blebbing (77). ROCK causes phosphorylation of myosin regulatory light chain, which controls actomyosin filament assembly and contraction (97, 98). Bleb formation is regulated by contraction of actomyosin filaments, as this causes their detachment from the plasma membrane. We also show that blebbing is a reversible process, with retraction occurring after removal of extracellular ATP. These results distinguish P2X7-induced blebbing in macrophages from irreversible apoptotic blebbing (99).

Phosphatidylserine translation from the inner to the outer plasma membrane leaflet occurs rapidly after P2X7R stimulation (2). This fast phospholipid redistribution acts as a non-apoptotic signaling mechanism in lymphocytes that serves to regulate the activity of several membrane proteins. For instance, PS switch modulates Ca^{2+} and Na^+ flux through the P2X7R, P2X7R-mediated shedding of the homing receptor CD62L, and inhibits the activity of the transporter P-glycoprotein (100). Here we show that P2X7R-induced PS switch relies upon Cl^- channel activation, and this process is independent of Ca^{2+} flux. Again, silencing Ano6 does not prevent PS flip. Based on these results, we speculate that a separate anoctamin family member may act as the scramblase downstream of the P2X7R. In support of this view, several other anoctamin family members, including Ano3, Ano 4, Ano 7, and Ano 10 also function as phospholipid scramblases (101). Future studies should investigate the expression and contribution of these channels to human macrophage PS switch.

Although a role for Cl^- flux in mediating NLRP3 inflammasome activity was recently reported (84, 102), the signaling cascade between ion flux and cytokine release is poorly understood. Previous reports indicate that mitochondrial ROS production is necessary for CLICs-dependent IL-1β release in mouse macrophages and THP-1 cells (84). In contrast, our results show that ROS production does not occur downstream of P2X7R activation in primary human macrophages under the conditions of our experiments. Moreover, the CLICs inhibitor IAA-94 did not prevent P2X7R mediated caspase-1 activation. Thus, our results suggest that inflammasome activation is independent of ROS generation and CLICs in primary human macrophages. However, P2X7R-induced caspase-1 activation and IL-1β release do require Cl^- channel stimulation in human macrophages, as tannic acid and A01 block these processes. Our data agree with a recent report in murine macrophages that established tannic acid acts as a potent inhibitor of the NLRP3 inflammasome (103). The authors found that tannic acid inhibits LPS-induced NF-κB signaling, which ultimately blocks transcription of NLRP3 and IL-1β. Thus, the Cl^- channel required for IL-1β release in human macrophages may be responsible for driving NF-κB signaling. There is evidence that efflux of Cl^- promotes NEK7–NLRP3 interaction (84). NEK7 is a newly identified NLRP3-binding protein that acts downstream of K^+ efflux to regulate NLRP3 oligomerization and activation (104). Therefore, investigating whether Cl^- channels mediate NEK7–NLRP3 interaction in human macrophages is warranted.

Collectively, our results demonstrate that Cl^- channels act downstream of P2X7Rs and serve as central mediators of several innate immune functions in primary human macrophages. These Cl^- channels are stimulated by PLA_2 activation, an enzyme known to promote the production of many inflammatory mediators. The present data attribute several pro-inflammatory functions to P2X7Rs in human immune cells and suggest that targeting this pathway may be therapeutically useful in cases of IL-1β mediated disease.

Supplementary Material

Refer to Web version on PubMed Central for supplementary material.

Acknowledgements:

The authors thank the generous blood donors whose contributions made this work possible.

Supported by grants from the NIH (1R01GM112188) and the Saint Louis University School of Medicine.

Abbreviations:

BzATP:	3′-*O*- (4-benzoylbenzoyl) ATP
ECS:	Extracellular solution
FasL:	Fas ligand
IL-1β:	Interleukin 1 beta
IL-18:	Interleukin 18
MAPK:	Mitogen-activated protein kinase
NO:	Nitric Oxide
P2XRs:	P2 family of ionotropic nucleotide receptors
PLA_2:	Phospholipase A_2
PS:	Phosphatidylserine
ROCK:	Rho-associated, coiled-coil containing protein kinase
ROS:	Reactive oxygen species

References

1. Chiozzi P, Sanz JM, Ferrari D, Falzoni S, Aleotti A, Buell GN, Collo G, and Di Virgilio F. 1997 Spontaneous cell fusion in macrophage cultures expressing high levels of the P2Z/P2X7 receptor [published erratum appears in J Cell Biol 1997 Oct 20;139(2):following 571]. J Cell Biol 138: 697–706. [PubMed: 9245796]
2. de Torre-Minguela C, Barbera-Cremades M, Gomez AI, Martin-Sanchez F, and Pelegrin P. 2016 Macrophage activation and polarization modify P2X7 receptor secretome influencing the inflammatory process. Scientific reports 6: 22586. [PubMed: 26935289]
3. Csoka B, Nemeth ZH, Toro G, Idzko M, Zech A, Koscso B, Spolarics Z, Antonioli L, Cseri K, Erdelyi K, Pacher P, and Hasko G. 2015 Extracellular ATP protects against sepsis through

macrophage P2X7 purinergic receptors by enhancing intracellular bacterial killing. FASEB journal : official publication of the Federation of American Societies for Experimental Biology 29: 3626–3637. [PubMed: 26060214]

4. Moreira-Souza ACA, Almeida-da-Silva CLC, Rangel TP, Rocha GDC, Bellio M, Zamboni DS, Vommaro RC, and Coutinho-Silva R. 2017 The P2X7 Receptor Mediates Toxoplasma gondii Control in Macrophages through Canonical NLRP3 Inflammasome Activation and Reactive Oxygen Species Production. Frontiers in immunology 8: 1257. [PubMed: 29075257]
5. North RA 2002 Molecular physiology of P2X receptors. Physiol Rev 82: 1013–1067. [PubMed: 12270951]
6. Pellegatti P, Raffaghello L, Bianchi G, Piccardi F, Pistoia V, and Di Virgilio F. 2008 Increased level of extracellular ATP at tumor sites: in vivo imaging with plasma membrane luciferase. PLoS ONE 3: e2599. [PubMed: 18612415]
7. Wilhelm K, Ganesan J, Muller T, Durr C, Grimm M, Beilhack A, Krempl CD, Sorichter S, Gerlach UV, Juttner E, Zerweck A, Gartner F, Pellegatti P, Di Virgilio F, Ferrari D, Kambham N, Fisch P, Finke J, Idzko M, and Zeiser R. 2010 Graft-versus-host disease is enhanced by extracellular ATP activating P2X7R. Nat. Med 16: 1434–1438. [PubMed: 21102458]
8. Di Virgilio F, Dal Ben D, Sarti AC, Giuliani AL, and Falzoni S. 2017 The P2X7 Receptor in Infection and Inflammation. Immunity 47: 15–31. [PubMed: 28723547]
9. Yang D, He Y, Munoz-Planillo R, Liu Q, and Nunez G. 2015 Caspase-11 Requires the Pannexin-1 Channel and the Purinergic P2X7 Pore to Mediate Pyroptosis and Endotoxic Shock. Immunity 43: 923–932. [PubMed: 26572062]
10. Seman M, Adriouch S, Scheuplein F, Krebs C, Freese D, Glowacki G, Deterre P, Haag F, and Koch-Nolte F. 2003 NAD-induced T cell death: ADP-ribosylation of cell surface proteins by ART2 activates the cytolytic P2X7 purinoceptor. Immunity 19: 571–582. [PubMed: 14563321]
11. Rissiek B, Danquah W, Haag F, and Koch-Nolte F. 2014 Technical Advance: a new cell preparation strategy that greatly improves the yield of vital and functional Tregs and NKT cells. Journal of leukocyte biology 95: 543–549. [PubMed: 24212099]
12. Sanz JM, Chiozzi P, Ferrari D, Colaianna M, Idzko M, Falzoni S, Fellin R, Trabace L, and Di Virgilio F. 2009 Activation of microglia by amyloid {beta} requires P2X7 receptor expression. J Immunol 182: 4378–4385. [PubMed: 19299738]
13. Niemi K, Teirila L, Lappalainen J, Rajamaki K, Baumann MH, Oorni K, Wolff H, Kovanen PT, Matikainen S, and Eklund KK. 2011 Serum amyloid A activates the NLRP3 inflammasome via P2X7 receptor and a cathepsin B-sensitive pathway. J Immunol 186: 6119–6128. [PubMed: 21508263]
14. Elssner A, Duncan M, Gavrilin M, and Wewers MD. 2004 A novel P2X7 receptor activator, the human cathelicidin-derived peptide LL37, induces IL-1 beta processing and release. J Immunol 172: 4987–4994. [PubMed: 15067080]
15. Tomasinsig L, Pizzirani C, Skerlavaj B, Pellegatti P, Gulinelli S, Tossi A, Di Virgilio F, and Zanetti M. 2008 The human cathelicidin LL-37 modulates the activities of the P2X7 receptor in a structure-dependent manner. J Biol Chem
16. Kerur N, Hirano Y, Tarallo V, Fowler BJ, Bastos-Carvalho A, Yasuma T, Yasuma R, Kim Y, Hinton DR, Kirschning CJ, Gelfand BD, and Ambati J. 2013 TLR-independent and P2X7-dependent signaling mediate Alu RNA-induced NLRP3 inflammasome activation in geographic atrophy. Investigative ophthalmology & visual science 54: 7395–7401. [PubMed: 24114535]
17. Fowler BJ, Gelfand BD, Kim Y, Kerur N, Tarallo V, Hirano Y, Amarnath S, Fowler DH, Radwan M, Young MT, Pittman K, Kubes P, Agarwal HK, Parang K, Hinton DR, Bastos-Carvalho A, Li S, Yasuma T, Mizutani T, Yasuma R, Wright C, and Ambati J. 2014 Nucleoside reverse transcriptase inhibitors possess intrinsic anti-inflammatory activity. Science 346: 1000–1003. [PubMed: 25414314]
18. Di Virgilio F 2007 Liaisons dangereuses: P2X(7) and the inflammasome. Trends Pharmacol Sci 28: 465–472. [PubMed: 17692395]
19. Qiu S, Liu J, and Xing F. 2017 ‘Hints’ in the killer protein gasdermin D: unveiling the secrets of gasdermins driving cell death. Cell death and differentiation 24: 588–596. [PubMed: 28362726]

20. Evavold CL, Ruan J, Tan Y, Xia S, Wu H, and Kagan JC. 2018 The Pore-Forming Protein Gasdermin D Regulates Interleukin-1 Secretion from Living Macrophages. Immunity 48: 35–44 e36. [PubMed: 29195811]
21. Sims JE, and Smith DE. 2010 The IL-1 family: regulators of immunity. Nature reviews. Immunology 10: 89–102.
22. Tapper H 1996 The secretion of preformed granules by macrophages and neutrophils. Journal of leukocyte biology 59: 613–622. [PubMed: 8656045]
23. Pfeiffer ZA, Aga M, Prabhu U, Watters JJ, Hall DJ, and Bertics PJ. 2004 The nucleotide receptor P2X7 mediates actin reorganization and membrane blebbing in RAW 264.7 macrophages via p38 MAP kinase and Rho. J Leukoc Biol
24. Jiang LH, Rassendren F, Mackenzie A, Zhang YH, Surprenant A, and North RA. 2005 N-methyl-D-glucamine and propidium dyes utilize different permeation pathways at rat P2X(7) receptors. Am J Physiol Cell Physiol 289: C1295–1302. [PubMed: 16093280]
25. Taylor SR, Gonzalez-Begne M, Dewhurst S, Chimini G, Higgins CF, Melvin JE, and Elliott JI. 2008 Sequential shrinkage and swelling underlie P2X7-stimulated lymphocyte phosphatidylserine exposure and death. J Immunol 180: 300–308. [PubMed: 18097031]
26. Sluyter R, Shemon AN, and Wiley JS. 2007 P2X(7) receptor activation causes phosphatidylserine exposure in human erythrocytes. Biochem Biophys Res Commun 355: 169–173. [PubMed: 17286963]
27. Courageot MP, Lepine S, Hours M, Giraud F, and Sulpice JC. 2004 Involvement of sodium in early phosphatidylserine exposure and phospholipid scrambling induced by P2X7 purinoceptor activation in thymocytes. J Biol Chem 279: 21815–21823. [PubMed: 14996828]
28. Ravichandran KS 2011 Beginnings of a good apoptotic meal: the find-me and eat-me signaling pathways. Immunity 35: 445–455. [PubMed: 22035837]
29. Segawa K, and Nagata S. 2015 An Apoptotic 'Eat Me' Signal: Phosphatidylserine Exposure. Trends Cell Biol 25: 639–650. [PubMed: 26437594]
30. Mackenzie AB, Young MT, Adinolfi E, and Surprenant A. 2005 Pseudoapoptosis induced by brief activation of ATP-gated P2X7 receptors. J Biol Chem 280: 33968–33976. [PubMed: 15994333]
31. Pelegrin P 2011 Many ways to dilate the P2X7 receptor pore. Br J Pharmacol 163: 908–911. [PubMed: 21410461]
32. Di Virgilio F, Schmalzing G, and Markwardt F. 2018 The Elusive P2X7 Macropore. Trends Cell Biol
33. Yan Z, Khadra A, Li S, Tomic M, Sherman A, and Stojilkovic SS. 2010 Experimental characterization and mathematical modeling of P2X7 receptor channel gating. J Neurosci 30: 14213–14224. [PubMed: 20962242]
34. Yaron JR, Gangaraju S, Rao MY, Kong X, Zhang L, Su F, Tian Y, Glenn HL, and Meldrum DR. 2015 K(+) regulates Ca(2+) to drive inflammasome signaling: dynamic visualization of ion flux in live cells. Cell death & disease 6: e1954. [PubMed: 26512962]
35. Pelegrin P, and Surprenant A. 2006 Pannexin-1 mediates large pore formation and interleukin-1beta release by the ATP-gated P2X7 receptor. Embo J 25: 5071–5082. [PubMed: 17036048]
36. Gavet O, and Pines J. 2010 Progressive activation of CyclinB1-Cdk1 coordinates entry to mitosis. Dev Cell 18: 533–543. [PubMed: 20412769]
37. Donnelly-Roberts DL, Namovic MT, Faltynek CR, and Jarvis MF. 2004 Mitogen-activated protein kinase and caspase signaling pathways are required for P2X7 receptor (P2X7R)-induced pore formation in human THP-1 cells. J Pharmacol Exp Ther 308: 1053–1061. [PubMed: 14634045]
38. Faria RX, Defarias FP, and Alves LA. 2005 Are second messengers crucial for opening the pore associated with P2X7 receptor? Am J Physiol Cell Physiol 288: C260–271. [PubMed: 15469955]
39. Marques-da-Silva C, Chaves MM, Castro NG, Coutinho-Silva R, and Guimaraes MZ. 2011 Colchicine inhibits cationic dye uptake induced by ATP in P2X2 and P2X7 receptor-expressing cells: implications for its therapeutic action. Br J Pharmacol 163: 912–926. [PubMed: 21306580]
40. Virginio C, MacKenzie A, North RA, and Surprenant A. 1999 Kinetics of cell lysis, dye uptake and permeability changes in cells expressing the rat P2X7 receptor. J Physiol 519 Pt 2: 335–346. [PubMed: 10457053]

41. Liang X, Samways DS, Wolf K, Bowles EA, Richards JP, Bruno J, Dutertre S, DiPaolo RJ, and Egan TM. 2015 Quantifying Ca2+ Current and Permeability in ATP-gated P2X7 Receptors. J Biol Chem 290: 7930–7942. [PubMed: 25645917]
42. Edelstein A, Amodaj N, Hoover K, Vale R, and Stuurman N. 2010 Computer control of microscopes using microManager. Current protocols in molecular biology / *edited by* Ausubel Frederick M.... [et al.] Chapter 14: Unit 14 20.
43. Schindelin J, Arganda-Carreras I, Frise E, Kaynig V, Longair M, Pietzsch T, Preibisch S, Rueden C, Saalfeld S, Schmid B, Tinevez JY, White DJ, Hartenstein V, Eliceiri K, Tomancak P, and Cardona A. 2012 Fiji: an open-source platform for biological-image analysis. Nat Methods 9: 676–682. [PubMed: 22743772]
44. Hazleton JE, Berman JW, and Eugenin EA. 2012 Purinergic receptors are required for HIV-1 infection of primary human macrophages. J Immunol 188: 4488–4495. [PubMed: 22450808]
45. Rassendren F, Buell GN, Virginio C, Collo G, North RA, and Surprenant A. 1997 The permeabilizing ATP receptor, P2X7. Cloning and expression of a human cDNA. J Biol Chem 272: 5482–5486. [PubMed: 9038151]
46. Eschke D, Wust M, Hauschildt S, and Nieber K. 2002 Pharmacological characterization of the P2X(7) receptor on human macrophages using the patch-clamp technique. Naunyn Schmiedebergs Arch Pharmacol 365: 168–171. [PubMed: 11819036]
47. Layhadi JA, and Fountain SJ. 2017 P2X4 Receptor-Dependent Ca(2+) Influx in Model Human Monocytes and Macrophages. Int J Mol Sci 18.
48. Layhadi JA, Turner J, Crossman D, and Fountain SJ. 2018 ATP Evokes Ca(2+) Responses and CXCL5 Secretion via P2X4 Receptor Activation in Human Monocyte-Derived Macrophages. J Immunol 200: 1159–1168. [PubMed: 29255078]
49. Norenberg W, Sobottka H, Hempel C, Plotz T, Fischer W, Schmalzing G, and Schaefer M. 2012 Positive allosteric modulation by ivermectin of human but not murine P2X7 receptors. Br J Pharmacol 167: 48–66. [PubMed: 22506590]
50. Seyffert C, Schmalzing G, and Markwardt F. 2004 Dissecting individual current components of co-expressed human P2X1 and P2X7 receptors. Curr Top Med Chem 4: 1719–1730. [PubMed: 15579104]
51. Wareham K, Vial C, Wykes RC, Bradding P, and Seward EP. 2009 Functional evidence for the expression of P2X1, P2X4 and P2X7 receptors in human lung mast cells. Br J Pharmacol 157: 1215–1224. [PubMed: 19552691]
52. Jarvis MF, and Khakh BS. 2009 ATP-gated P2X cation-channels. Neuropharmacology 56: 208–215. [PubMed: 18657557]
53. Chessell IP, Michel AD, and Humphrey PPA. 1997 Properties of the pore-forming P2X7 purinoceptor in mouse NTW8 microglial cells. Br J Pharmacol 121: 1429–1437. [PubMed: 9257924]
54. Roger S, Pelegrin P, and Surprenant A. 2008 Facilitation of P2X7 receptor currents and membrane blebbing via constitutive and dynamic calmodulin binding. J Neurosci 28: 6393–6401. [PubMed: 18562610]
55. Monif M, Reid CA, Powell KL, Drummond KJ, O'Brien TJ, and Williams DA. 2016 Interleukin-1beta has trophic effects in microglia and its release is mediated by P2X7R pore. Journal of neuroinflammation 13: 173. [PubMed: 27364756]
56. Napotnik TB 2016 Fluorescent Indicators of Membrane Permeabilization Due to Electroporation. In Handbook of Electroporation Miklavcic D, ed. Springer International Publishing, Cham 1–19.
57. Hickman SE, el Khoury J, Greenberg S, Schieren I, and Silverstein SC. 1994 P2Z adenosine triphosphate receptor activity in cultured human monocyte-derived macrophages. Blood 84: 2452–2456. [PubMed: 7919365]
58. Schachter J, Motta AP, de Souza Zamorano A, da Silva-Souza HA, Guimaraes MZ, and Persechini PM. 2008 ATP-induced P2X7-associated uptake of large molecules involves distinct mechanisms for cations and anions in macrophages. J Cell Sci 121: 3261–3270. [PubMed: 18782864]
59. Falzoni S, Munerati M, Ferrari D, Spisani S, Moretti S, and Di Virgilio F. 1995 The purinergic P2Z receptor of human macrophage cells. Characterization and possible physiological role. J Clin Invest 95: 1207–1216. [PubMed: 7883969]

60. Browne LE, Compan V, Bragg L, and North RA. 2013 P2X7 receptor channels allow direct permeation of nanometer-sized dyes. J Neurosci 33: 3557–3566. [PubMed: 23426683]
61. Karasawa A, Michalski K, Mikhelzon P, and Kawate T. 2017 The P2X7 receptor forms a dye-permeable pore independent of its intracellular domain but dependent on membrane lipid composition. eLife 6.
62. Steinberg TH, Newman AS, Swanson JA, and Silverstein SC. 1987 ATP4- permeabilizes the plasma membrane of mouse macrophages to fluorescent dyes. J Biol Chem 262: 8884–8888. [PubMed: 3597398]
63. Pelegrin P, and Surprenant A. 2007 Pannexin-1 couples to maitotoxin- and nigericin-induced interleukin-1beta release through a dye uptake-independent pathway. J Biol Chem 282: 2386–2394. [PubMed: 17121814]
64. Silverman WR, de Rivero Vaccari JP, Locovei S, Qiu F, Carlsson SK, Scemes E, Keane RW, and Dahl G. 2009 The pannexin 1 channel activates the inflammasome in neurons and astrocytes. J Biol Chem 284: 18143–18151. [PubMed: 19416975]
65. Ousingsawat J, Wanitchakool P, Kmit A, Romao AM, Jantarajit W, Schreiber R, and Kunzelmann K. 2015 Anoctamin 6 mediates effects essential for innate immunity downstream of P2X7 receptors in macrophages. Nat Commun 6: 6245. [PubMed: 25651887]
66. Kmit A, van Kruchten R, Ousingsawat J, Mattheij NJ, Senden-Gijsbers B, Heemskerk JW, Schreiber R, Bevers EM, and Kunzelmann K. 2013 Calcium-activated and apoptotic phospholipid scrambling induced by Ano6 can occur independently of Ano6 ion currents. Cell death & disease 4: e611. [PubMed: 23618909]
67. Pelegrin P, and Surprenant A. 2009 The P2X(7) receptor-pannexin connection to dye uptake and IL-1beta release. Purinergic Signal
68. Kim M, Jiang LH, Wilson HL, North RA, and Surprenant A. 2001 Proteomic and functional evidence for a P2X(7) receptor signalling complex. Embo J 20: 6347–6358. [PubMed: 11707406]
69. Costa-Junior HM, Mendes AN, Davis GH, da Cruz CM, Ventura AL, Serezani CH, Faccioli LH, Nomizo A, Freire-de-Lima CG, Bisaggio Rda C, and Persechini PM. 2009 ATP-induced apoptosis involves a Ca2+-independent phospholipase A2 and 5-lipoxygenase in macrophages. Prostaglandins Other Lipid Mediat 88: 51–61. [PubMed: 18984060]
70. Franchi L, Chen G, Marina-Garcia N, Abe A, Qu Y, Bao S, Shayman JA, Turk J, Dubyak GR, and Nunez G. 2009 Calcium-independent phospholipase A2 beta is dispensable in inflammasome activation and its inhibition by bromoenol lactone. Journal of innate immunity 1: 607–617. [PubMed: 20160900]
71. Leduc-Pessah H, Weilinger NL, Fan CY, Burma NE, Thompson RJ, and Trang T. 2017 Site-Specific Regulation of P2X7 Receptor Function in Microglia Gates Morphine Analgesic Tolerance. J Neurosci 37: 10154–10172. [PubMed: 28924009]
72. Ekokoski E, Dugue B, Vainio M, Vainio PJ, and Tornquist K. 2000 Extracellular ATP-mediated phospholipase A(2) activation in rat thyroid FRTL-5 cells: regulation by a G(i)/G(o) protein, Ca(2+), and mitogen-activated protein kinase. Journal of cellular physiology 183: 155–162. [PubMed: 10737891]
73. Bianco F, Perrotta C, Novellino L, Francolini M, Riganti L, Menna E, Saglietti L, Schuchman EH, Furlan R, Clementi E, Matteoli M, and Verderio C. 2009 Acid sphingomyelinase activity triggers microparticle release from glial cells. EMBO J 28: 1043–1054. [PubMed: 19300439]
74. MacKenzie A, Wilson HL, Kiss-Toth E, Dower SK, North RA, and Surprenant A. 2001 Rapid secretion of interleukin-1beta by microvesicle shedding. Immunity 15: 825–835. [PubMed: 11728343]
75. Babiychuk EB, Monastyrskaya K, Potez S, and Draeger A. 2011 Blebbing confers resistance against cell lysis. Cell Death Differ 18: 80–89. [PubMed: 20596076]
76. Verhoef PA, Estacion M, Schilling W, and Dubyak GR. 2003 P2X7 receptor-dependent blebbing and the activation of Rho-effector kinases, caspases, and IL-1 beta release. J Immunol 170: 5728–5738. [PubMed: 12759456]
77. Panupinthu N, Zhao L, Possmayer F, Ke HZ, Sims SM, and Dixon SJ. 2007 P2X7 nucleotide receptors mediate blebbing in osteoblasts through a pathway involving lysophosphatidic acid. J Biol Chem 282: 3403–3412. [PubMed: 17135244]

78. Rathinam VA, and Fitzgerald KA. 2016 Inflammasome Complexes: Emerging Mechanisms and Effector Functions. Cell 165: 792–800. [PubMed: 27153493]

79. Shi J, Zhao Y, Wang K, Shi X, Wang Y, Huang H, Zhuang Y, Cai T, Wang F, and Shao F. 2015 Cleavage of GSDMD by inflammatory caspases determines pyroptotic cell death. Nature 526: 660–665. [PubMed: 26375003]

80. Giuliani AL, Sarti AC, Falzoni S, and Di Virgilio F. 2017 The P2X7 Receptor-Interleukin-1 Liaison. Frontiers in pharmacology 8: 123. [PubMed: 28360855]

81. Di Virgilio F, Sarti AC, and Grassi F. 2018 Modulation of innate and adaptive immunity by P2X ion channels. Curr Opin Immunol 52: 51–59. [PubMed: 29631184]

82. Schreiber R, Ousingsawat J, Wanitchakool P, Sirianant L, Benedetto R, Reiss K, and Kunzelmann K. 2018 Regulation of TMEM16A/ANO1 and TMEM16F/ANO6 ion currents and phospholipid scrambling by Ca(2+) and plasma membrane lipid. J Physiol 596: 217–229. [PubMed: 29134661]

83. Argenzio E, and Moolenaar WH. 2016 Emerging biological roles of Cl- intracellular channel proteins. J Cell Sci 129: 4165–4174. [PubMed: 27852828]

84. Tang T, Lang X, Xu C, Wang X, Gong T, Yang Y, Cui J, Bai L, Wang J, Jiang W, and Zhou R. 2017 CLICs-dependent chloride efflux is an essential and proximal upstream event for NLRP3 inflammasome activation. Nature communications 8: 202.

85. Gordon S, and Martinez-Pomares L. 2017 Physiological roles of macrophages. Pflugers Arch 469: 365–374. [PubMed: 28185068]

86. Marques-da-Silva C, Chaves MM, Chaves SP, Figliuolo VR, Meyer-Fernandes JR, Corte-Real S, Lameu C, Ulrich H, Ojcius DM, Rossi-Bergmann B, and Coutinho-Silva R. 2011 Infection with Leishmania amazonensis upregulates purinergic receptor expression and induces host-cell susceptibility to UTP-mediated apoptosis. Cell Microbiol 13: 1410–1428. [PubMed: 21740498]

87. Marques-da-Silva C, Chaves MM, Rodrigues JC, Corte-Real S, Coutinho-Silva R, and Persechini PM. 2011 Differential modulation of ATP-induced P2X7-associated permeabilities to cations and anions of macrophages by infection with Leishmania amazonensis. PLoS ONE 6: e25356. [PubMed: 21966508]

88. Zhang YH, He M, Wang Y, and Liao AH. 2017 Modulators of the Balance between M1 and M2 Macrophages during Pregnancy. Front Immunol 8: 120. [PubMed: 28232836]

89. Yu K, Whitlock JM, Lee K, Ortlund EA, Cui YY, and Hartzell HC. 2015 Identification of a lipid scrambling domain in ANO6/TMEM16F. Elife 4: e06901. [PubMed: 26057829]

90. Oh U, and Jung J. 2016 Cellular functions of TMEM16/anoctamin. Pflugers Arch 468: 443–453. [PubMed: 26811235]

91. Yang H, Kim A, David T, Palmer D, Jin T, Tien J, Huang F, Cheng T, Coughlin SR, Jan YN, and Jan LY. 2012 TMEM16F forms a Ca2+-activated cation channel required for lipid scrambling in platelets during blood coagulation. Cell 151: 111–122. [PubMed: 23021219]

92. He Y, Hara H, and Nunez G. 2016 Mechanism and Regulation of NLRP3 Inflammasome Activation. Trends Biochem. Sci 41: 1012–1021. [PubMed: 27669650]

93. Akerboom J, Chen TW, Wardill TJ, Tian L, Marvin JS, Mutlu S, Calderon NC, Esposti F, Borghuis BG, Sun XR, Gordus A, Orger MB, Portugues R, Engert F, Macklin JJ, Filosa A, Aggarwal A, Kerr RA, Takagi R, Kracun S, Shigetomi E, Khakh BS, Baier H, Lagnado L, Wang SS, Bargmann CI, Kimmel BE, Jayaraman V, Svoboda K, Kim DS, Schreiter ER, and Looger LL. 2012 Optimization of a GCaMP calcium indicator for neural activity imaging. J Neurosci 32: 13819–13840. [PubMed: 23035093]

94. Whitlock JM, and Hartzell HC. 2016 A Pore Idea: the ion conduction pathway of TMEM16/ANO proteins is composed partly of lipid. Pflugers Arch 468: 455–473. [PubMed: 26739711]

95. Ousingsawat J, Wanitchakool P, Schreiber R, and Kunzelmann K. 2018 Contribution of TMEM16F to pyroptotic cell death. Cell death & disease 9: 300. [PubMed: 29463790]

96. Sirianant L, Ousingsawat J, Wanitchakool P, Schreiber R, and Kunzelmann K. 2016 Cellular volume regulation by anoctamin 6: Ca(2)(+), phospholipase A2 and osmosensing. Pflugers Arch 468: 335–349. [PubMed: 26438191]

97. Leverrier Y, and Ridley AJ. 2001 Apoptosis: caspases orchestrate the ROCK ‘n’ bleb. Nat Cell Biol 3: E91–93. [PubMed: 11283625]

98. Coleman ML, Sahai EA, Yeo M, Bosch M, Dewar A, and Olson MF. 2001 Membrane blebbing during apoptosis results from caspase-mediated activation of ROCK I. Nat Cell Biol 3: 339–345. [PubMed: 11283606]

99. Khajah MA, and Luqmani YA. 2016 Involvement of Membrane Blebbing in Immunological Disorders and Cancer. Med Princ Pract 25 Suppl 2: 18–27.

100. Elliott JI, Surprenant A, Marelli-Berg FM, Cooper JC, Cassady-Cain RL, Wooding C, Linton K, Alexander DR, and Higgins CF. 2005 Membrane phosphatidylserine distribution as a non-apoptotic signalling mechanism in lymphocytes. Nat Cell Biol 7: 808–816. [PubMed: 16025105]

101. Suzuki J, Fujii T, Imao T, Ishihara K, Kuba H, and Nagata S. 2013 Calcium-dependent phospholipid scramblase activity of TMEM16 protein family members. J Biol Chem 288: 13305–13316. [PubMed: 23532839]

102. Verhoef PA, Kertesy SB, Lundberg K, Kahlenberg JM, and Dubyak GR. 2005 Inhibitory effects of chloride on the activation of caspase-1, IL-1beta secretion, and cytolysis by the P2X7 receptor. J Immunol 175: 7623–7634. [PubMed: 16301672]

103. Song D, Zhao J, Deng W, Liao Y, Hong X, and Hou J. 2018 Tannic acid inhibits NLRP3 inflammasome-mediated IL-1beta production via blocking NF-kappaB signaling in macrophages. Biochem Biophys Res Commun 503: 3078–3085. [PubMed: 30126633]

104. He Y, Zeng MY, Yang D, Motro B, and Nunez G. 2016 NEK7 is an essential mediator of NLRP3 activation downstream of potassium efflux. Nature 530: 354–357. [PubMed: 26814970]

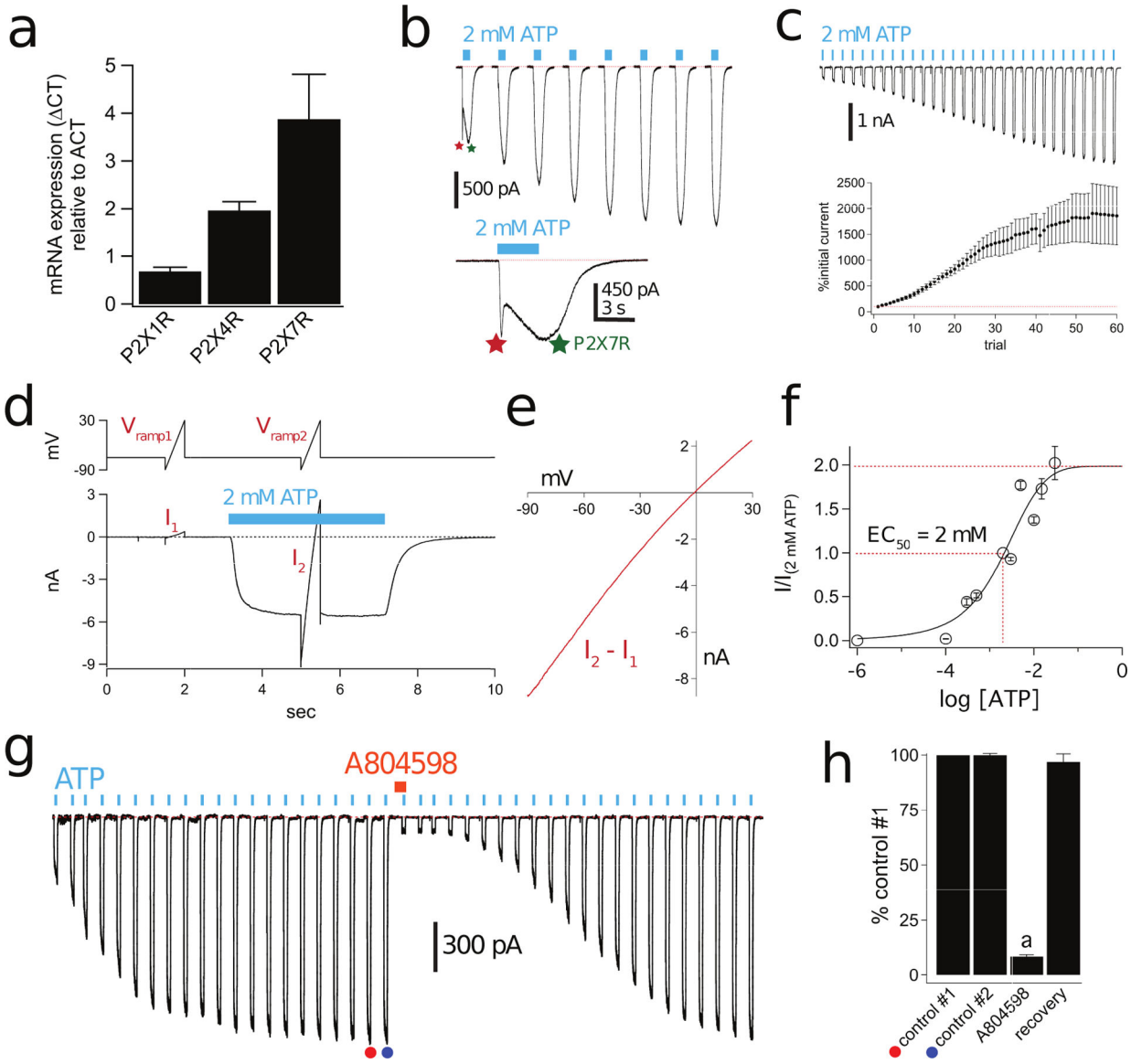

Figure 1. Human macrophages express facilitating P2X7Rs.

(a) RT-qPCR on total RNA isolated from human macrophages (n = 3 donors). The housekeeping gene β-actin (ACT) was used as an internal control of integrity of the samples. **(b)** Representative tracings of whole-cell currents (holding voltage = −60 mV) activated by 3s applications of 2 mM ATP (cyan bars) to a human macrophage; the time between consecutive applications was 15s. The first pulse of ATP produced a current that displayed two distinct phases; the first (red asterisk) is a desensitizing P2XR current, and the second (green asterisk) is a sustained current. The second application of ATP showed a smaller desensitizing current, and all further applications showed only the sustained current. Inset shows a close-up of the biphasic current caused by the first ATP application. **(c)** *Top*, Representative tracing of facilitating macrophage currents activated by 2 mM ATP. The figure shows 5 s of current recording for each application of ATP applied every 15 s. Consecutive traces are truncated to save space and more clearly show current facilitation.

Bottom, Mean ± s.e.m. of peak current amplitude normalized as the percentage of initial current for 60 ATP applications. **(d)** Representative fully facilitated current with voltage-ramp pulses from −90 mV to +30 mV. The holding potential was −60 mV. The rapid (a few μs) capacitive transients resulting from sudden voltage jumps were removed. The ATP-gated current was obtained by subtracting I_1, obtained in the absence of ATP, from I_2, obtained in the presence of ATP. **(e)** Current-voltage curve obtained from the data of Panel "d". The reversal potential near 0 mV suggests a non-selective current **(f)** Concentration-response curve for ATP in human macrophages. Repetitive applications of ATP were applied first to fully facilitate the current (not shown). Symbols are mean ± s.e.m. of the normalized current amplitude from 7 to 54 cells. Sigmoidal curve is the best fit obtained with a four-parameter logistic function. **(g)** Representative inhibition and recovery of facilitated current after a 2 min incubation (orange bar) in 1 μM of the P2X7R antagonist A804598. The concentration of ATP was 2 mM. **(h)** ATP-gated current amplitude as fraction of control #2. Data obtained from peak current amplitude experiments like that of Panel "g". The fact that control #2 (filled blue circle) is the same amplitude as control #1 (filled orange circle) shows that facilitation of the ATP-gated current was complete before administration of the antagonist. Current is significantly inhibited by the P2X7R antagonist, A804598 (1 μM, $n = 9$; $p < 0.0001$; paired *t*-test).

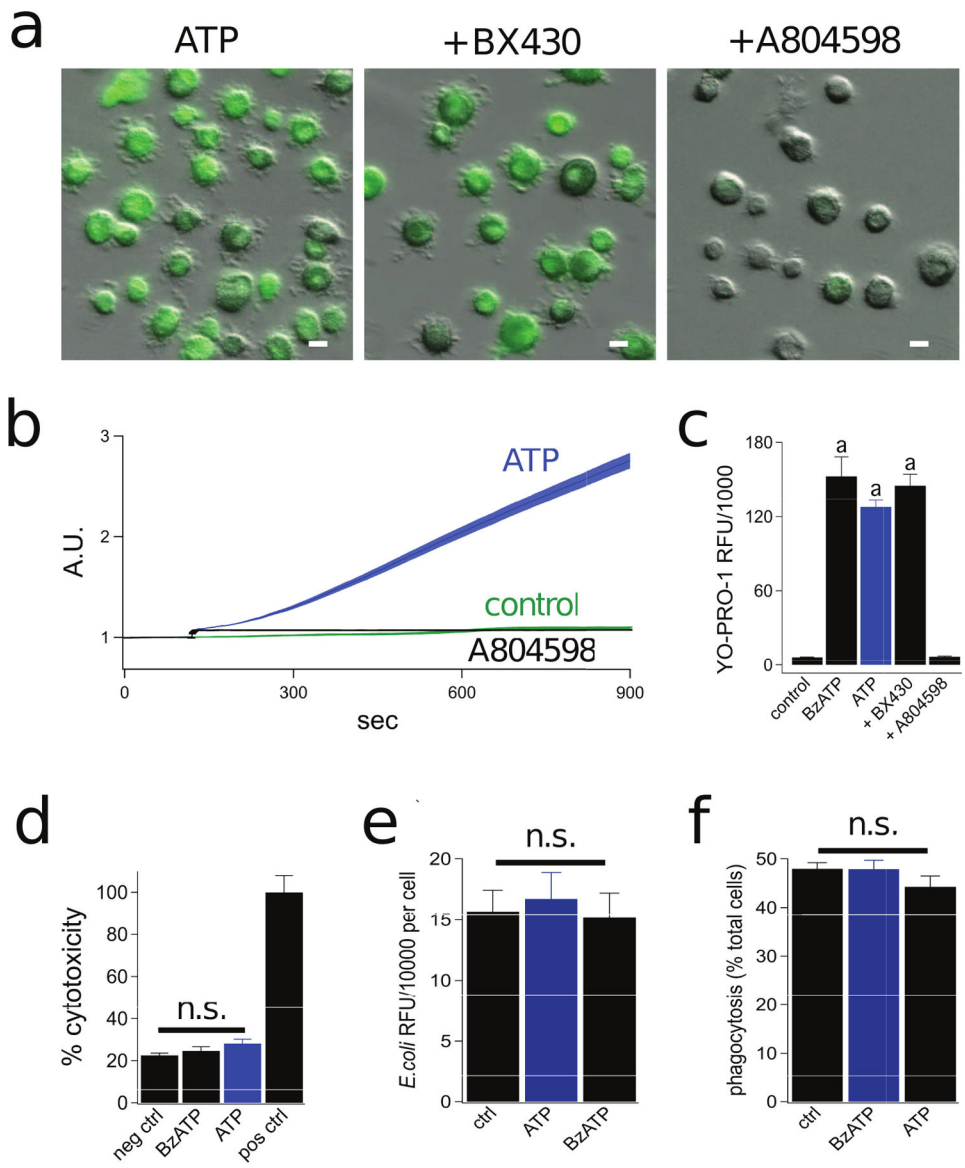

Figure 2. Stimulation of the P2X7R causes robust permeabilization of human macrophages.

(a) Representative fluorescence images of cells incubated for 15 min in the presence of 2 mM ATP +/− the antagonists BX430 (2 μM, for P2X4R) or A804598 (1 μM, for P2X7R) at 37°C. Each antagonist was pre-incubated for 30 min. Scale bars: 20 μm **(b)** Time-course of YO-PRO-1 uptake shows the mean ± s.e.m. of fluorescence intensity over time measured from human macrophages. Significant uptake of YO-PRO-1 was measured in the presence (blue trace) but not the absence of 2 mM ATP (green trace). ATP-evoked YO-PRO-1 uptake was blocked by 1 μM A804598 (black trace). A.U. is arbitrary fluorescence units. N >100 for each condition. **(c)** Quantitative comparison of YO-PRO-1 uptake by macrophages. RFU was determined as described in *Methods and Materials*. Cells were incubated for 15 min with YO-PRO-1 and 300 μM BzATP or 2 mM ATP in the presence of BX430 (2 μM) or A804598 (1 μM). Each antagonist was pre-incubated for 30 min. We measured significant inhibition of YO-PRO-1 uptake by A804598 (n = 6; $p < 0.0001$; ANOVA). “a” denotes

significant difference ($p > 0.001$) from control. **(d)** Human macrophages were treated with BzATP (300 μM) or ATP (2 mM) for 30 min at 37°C. The negative control was obtained from untreated macrophages and the positive control was from lysed macrophages. After treatment, cell supernatants were collected and LDH release was quantified. Percent cytotoxicity is the amount of LDH release normalized to the positive control. We measured no significant difference (n.s.) between the negative control and BzATP or ATP treated macrophages (n = 4 separate experiments). **(e)** Human macrophages incubated with 40 μg/mL pHrodo Red *E. coli* BioParticles at 37°C displayed strong spontaneous ingestion of *E. coli* that was not impacted by ATP (2 mM) or BzATP (300 μM); n = 4 experiments each. **(f)** Human macrophages exhibited robust spontaneous phagocytic capacity (48.0% of cells were *E. coli* positive) and this was not impacted by stimulation with ATP (44.3% of cells) or BzATP (47.9% of cells); n = 4 experiments each.

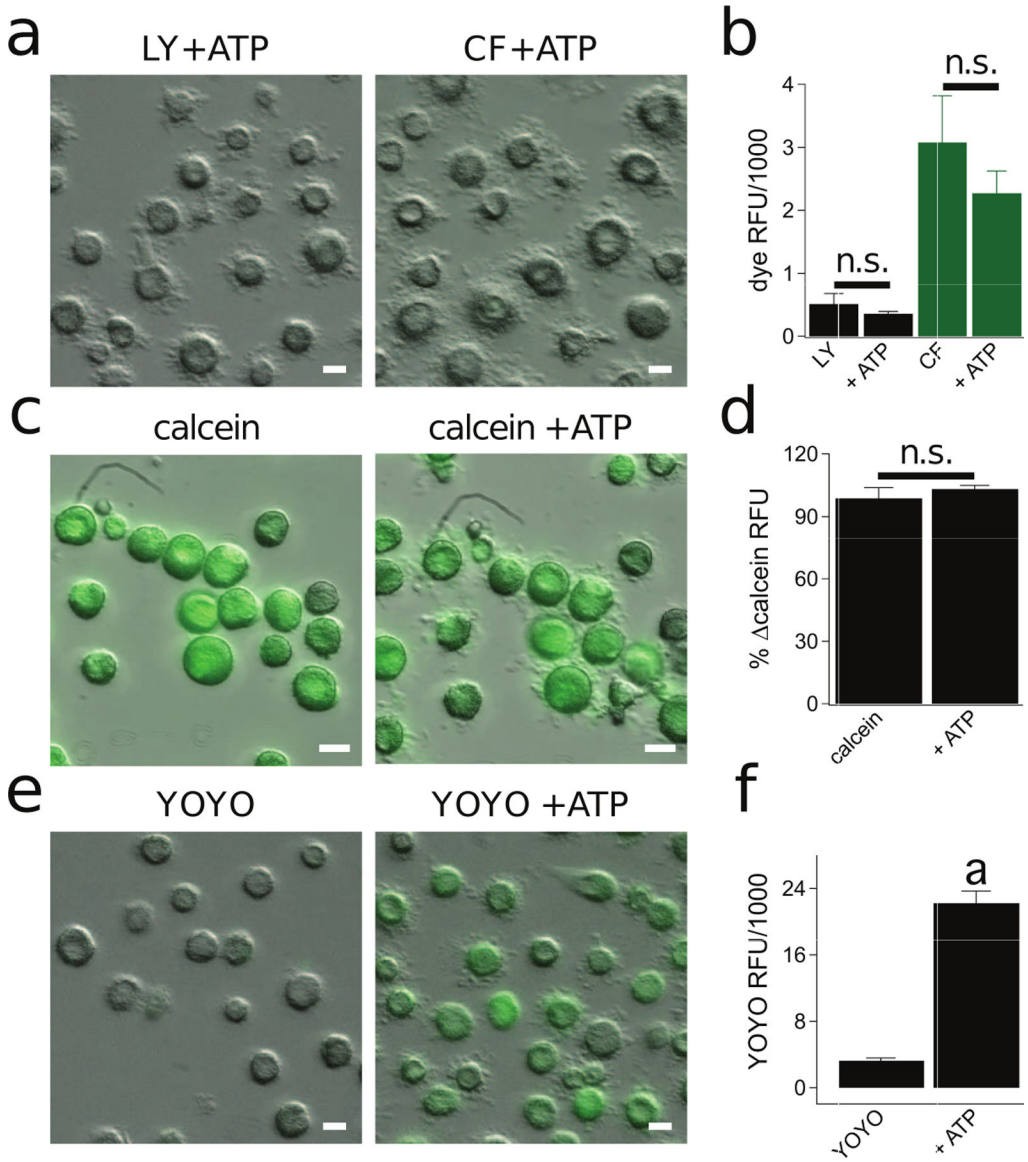

Figure 3. The P2X7R permeabilization pathway is cation selective.

(a) Fluorescence images of human macrophages incubated in the presence of ATP (2 mM) with the anionic dyes Lucifer yellow (LY, 0.5 mM) or carboxyfluorescein (CF, 0.5 mM) at 37°C. Scale bars: 20 μm. **(b)** Quantitative comparison of anionic dye uptake by macrophages. Cells were incubated for 15 min with LY or CF in the presence of ATP (2 mM) at 37°C. "n.s." are not significantly different from ATP (n = 4). **(c)** Fluorescence images of human macrophages preloaded with anionic calcein-AM (0.5 μM) for 30 min and subsequently stimulated with ATP (2 mM) for 15 min at 37°C. **(d)** Quantification of change in intracellular calcein fluorescence after 15 min stimulation with ATP (2 mM). There is no significant difference in fluorescence dye after ATP treatment (n = 4 separate experiments). **(e)** Fluorescence images of human macrophages incubated in the presence of ATP (2 mM) with the cationic dye YOYO-1 (5 μM) for 15 mins at 37°C. **(f)** Quantification of YOYO-1 after macrophages were incubated for 15 min with ATP (2 mM) at 37°C. There is significant

uptake of dye by ATP treated cells ($p < 0.0001$; unpaired t-test, n= 4 separate experiments). “a” is significantly different from control (i.e. YOYO-1 only).

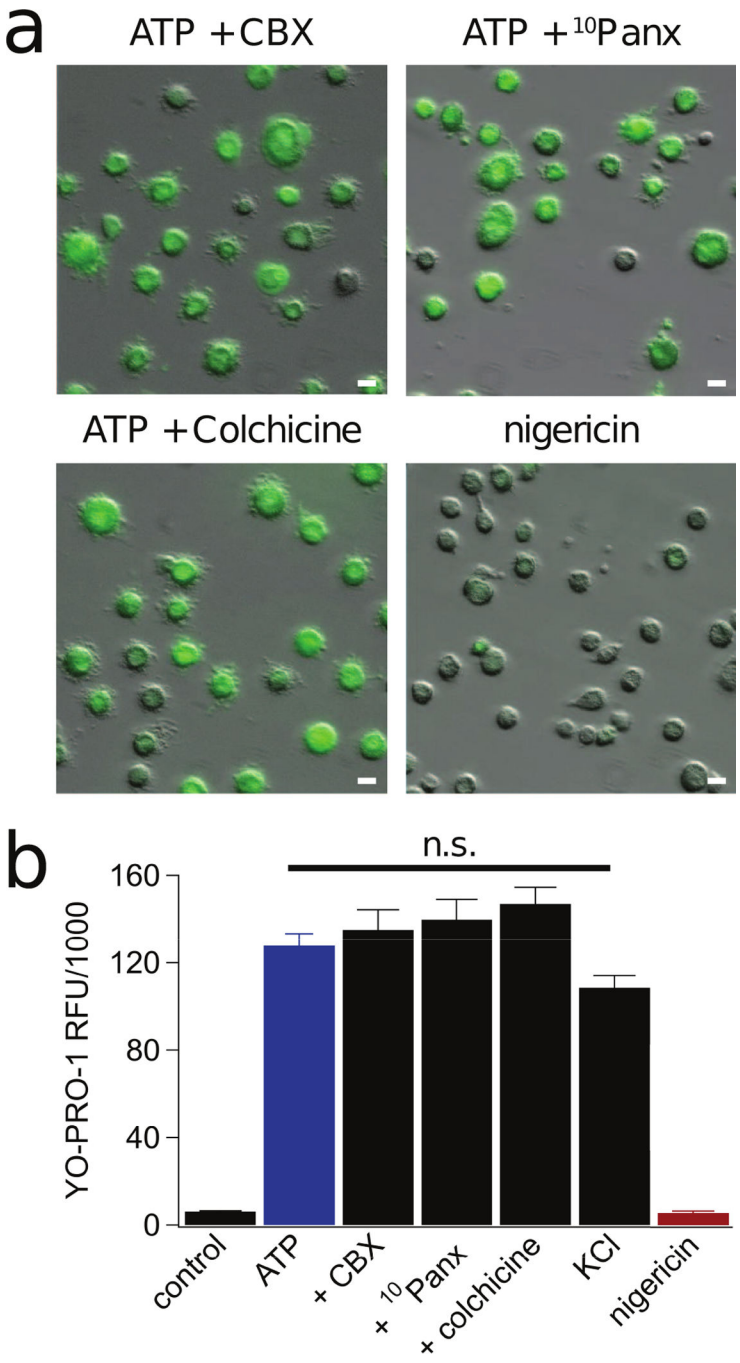

Figure 4. Pannexin-1 and microtubule stabilization are not involved in permeabilization of human macrophages.

(a) Macrophages were pre-incubated for 30 min with either the pannexin-1 inhibitors carbenoxolone (CBX, 20 μM) and ^{10}panx (300 μM) or colchicine (50 μM), and subsequently assessed for YO-PRO-1 uptake after 15 min of ATP (2 mM) at 37°C. None of the reagents prevented dye uptake (n = 5 separate experiments). Stimulation of macrophages with nigericin (20 μM) for 30 min did not promote uptake of YO-PRO-1 dye (n = 4 separate experiments). Scale bars: 20 μm. **(b)** Quantification of YO-PRO-1 fluorescence after

macrophages were incubated for 15 min with ATP (2 mM) +/− (CBX, 20 μM), ^{10}panx (300 μM), or colchicine (50 μM) in normal ECS; or with ATP (2 mM) in high K^+ ECS (130 mM KCl) at 37°C. We measured no significant inhibition of dye uptake from any treatment. YO-PRO-1 fluorescence after 30 min stimulation with nigericin (20 μM) for 30 min was not significantly different from untreated control macrophages. “n.s.” are not significantly different from ATP.

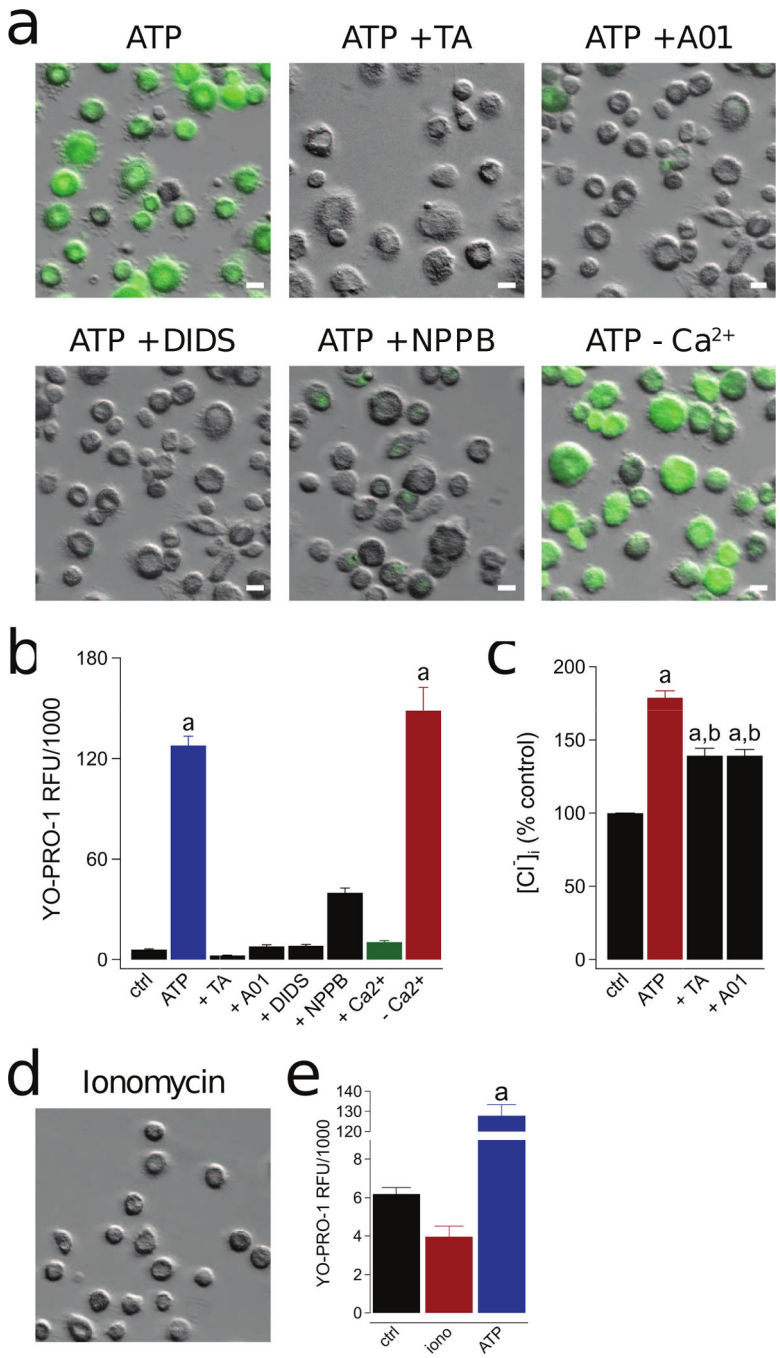

Figure 5. P2X7R-mediated activation of a Cl^- channel is responsible for human macrophage permeabilization.

(a) Representative images of macrophages pre-incubated for 30 min with the non-selective Cl^- channel inhibitors tannic acid (TA, 20 μM), A01 (40 μM), DIDS (100 μM), and NPPB (0.5 mM). YO-PRO-1 uptake was measured after 15 min in the presence of ATP (2 mM) in normal ECS at 37°C. The independence of YO-PRO-1 uptake on Ca^{2+} flux was assessed by loading the cells with 10 μM BAPTA-AM and measuring dye uptake in Ca^{2+} free ECS with 1 mM EDTA (-Ca^{2+}). Scale bars: 20 μm. **(b)** YO-PRO-1 fluorescence in Ca^{2+} free

conditions (-Ca^{2+}) was significantly different from control ("a" is equal to $p < 0.0001$; ANOVA) whereas uptake in the presence of four Cl^- channel antagonists was not. Dye uptake was inhibited by stimulating cells in ECS containing 2 mM Ca^{2+} (+Ca^{2+}; $p < 0.0001$; ANOVA). N = 4–7 separate experiments for all conditions. (**c**) Macrophages were pretreated with or without tannic acid (TA, 20 μM) or A01 (40 μM) for 30 mins and subsequently stimulated with or without ATP (2 mM) for 15 mins at 37°C. Supernatants were removed and replaced with dionized H_20. Intracellular chloride of cell lysates was measured with MQAE (100 μM) and normalized to untreated controls ("a" denotes a significant increase from control ($p<0.005$). "b" denotes a significant decrease from ATP ($p<0.005$), n=9 separate experiments). **(d)** Ionomycin (1 μM) causes no measurable YO-PRO-1 uptake. (**e**) No significant difference in YO-PRO-1 fluorescence between untreated control macrophages and those treated with ionomycin, n = 4 separate experiments. "a" indicates significant difference from control.

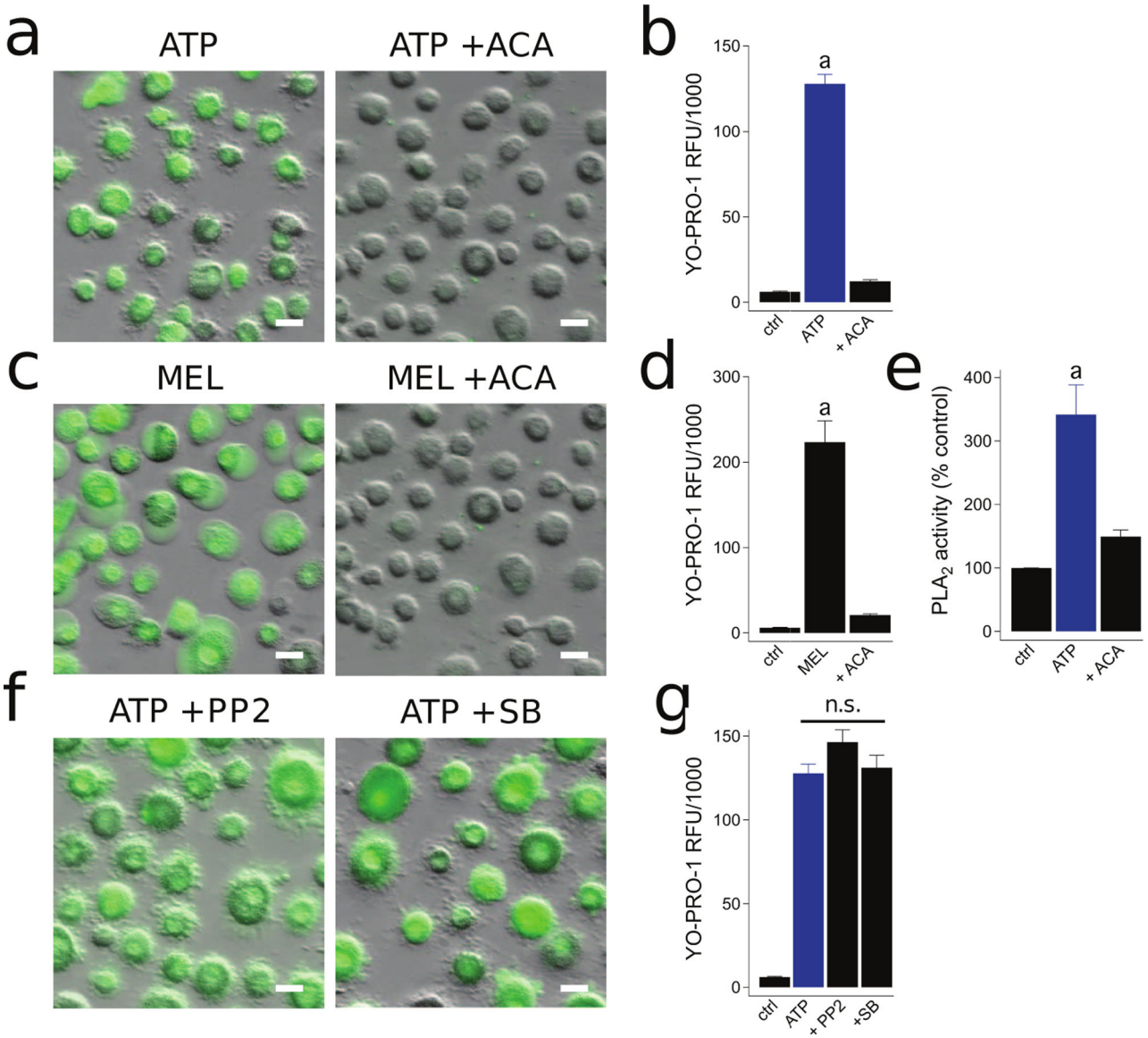

Figure 6. PLA_2 activation is required for P2X7R-mediated macrophage permeabilization.

(a) Macrophages were pre-incubated for 30 min with the PLA_2 inhibitor ACA (50 μM) and YO-PRO-1 uptake was measured after 15 min in the presence of ATP (2 mM) at 37°C. **(b)** ACA significantly inhibited YO-PRO-1 uptake; $p < 0.0001$; unpaired t-test, n = 4 separate experiments. “a” indicates significant difference from control. **(c)** YO-PRO uptake in macrophages incubated for 30 min in the presence of 10 μM Melittin (MEL) +/− ACA (50 μM) at 37°C. **(d)** MEL induced YO-PRO-1 fluorescence was significantly inhibited by ACA treatment; $p < 0.0001$; unpaired t-test, n = 4 separate experiments. **(e)** Macrophages were pretreated with or without ACA (50 μM) for 30 mins and subsequently stimulated with or without ATP (2 mM) for 15 mins at 37°C. PLA2 activity was measured with a colorimetric assay. The bar graph shows data normalized to nontreated control activity. “a” denotes a significant increase from control ($p<0.005$, n=5 separate experiments). **(f)** Macrophages pre-incubated for 30 min with the kinase inhibitors PP2 (20 μM) or SB-203580 (SB, 10 μM).

YO-PRO-1 uptake was measured after 15 min in the presence of ATP (2 mM) at 37°C. **(g)** YO-PRO-1 fluorescence was not significantly inhibited by PP2 or SB treatment. n = 4 separate experiments. Scale bars: 20 μm.

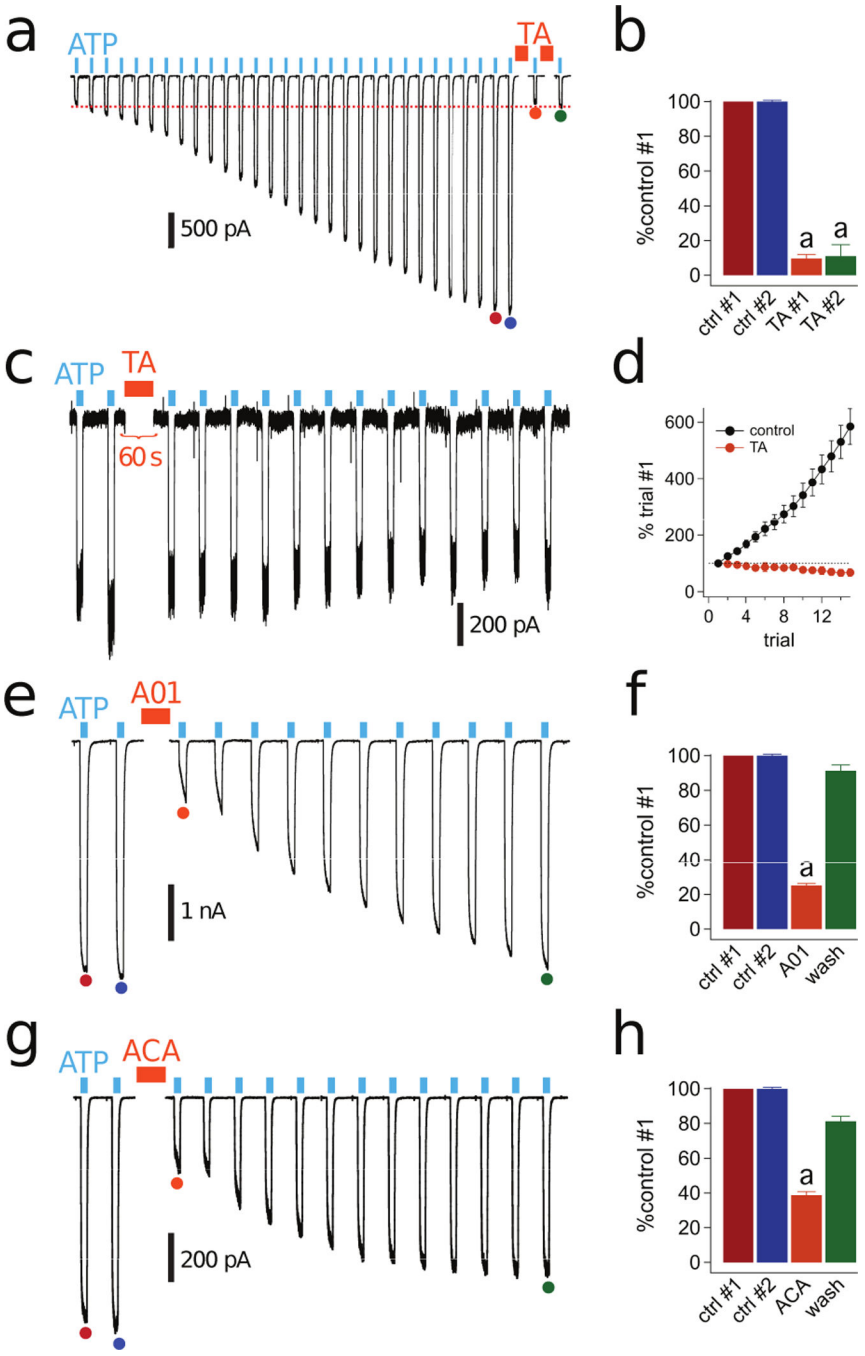

Figure 7. P2X7R facilitation is blocked by PLA_2 and Cl^- channel antagonists.

(a) An example of a facilitating whole-cell current activated by 2 mM ATP (cyan bars) in a human macrophage before and after 2-min incubation with 20 μM tannic acid (TA, orange bars) held at −60 mV. Traces were truncated as described in Fig 1. **(b)** The color of the bars reflect the positions of the currents indicated by the filled circles of the same colors in panel “a”. Current amplitude is shown as a percentage of control #1. The fact that controls #1 and #2 have the same amplitude indicate that the currents were fully facilitated before application of TA. The first application of tannic acid (TA #1, n=6 cells) significantly

inhibited facilitation ("a": $p < 0.01$; paired t-test). The current remaining after the first tannic acid application (TA #2) was not inhibited by a second 2-min tannic acid incubation period (n = 6 cells). **(c)** Representative tracing of macrophage ATP-gated current treated with tannic acid for 2 min after two 3 s applications of ATP and before facilitation occurs. Tannic acid prevented the development of facilitation under these conditions. **(d)** Current amplitude upon repetitive 3 s pulses of ATP every 15 s does not increase after tannic acid incubation (n=5 cells). **(e)** Representative tracing of fully-facilitated whole-cell currents activated by ATP before and after 2-min incubation with A01 (40 μM). **(f)** Current amplitude as the fraction of control #1 was significantly reduced in the presence of A01 (n=15 cells) ("a": $p < 0.0001$; unpaired t-test). **(g)** Representative tracing of fully-facilitated whole-cell currents activated by ATP before and after 2-min incubation with ACA (50 μM). **(h)** Current amplitude as the fraction of control #1 was significantly reduced in the presence of ACA (n=19 cells) ("a": $p < 0.0001$; unpaired t-test).

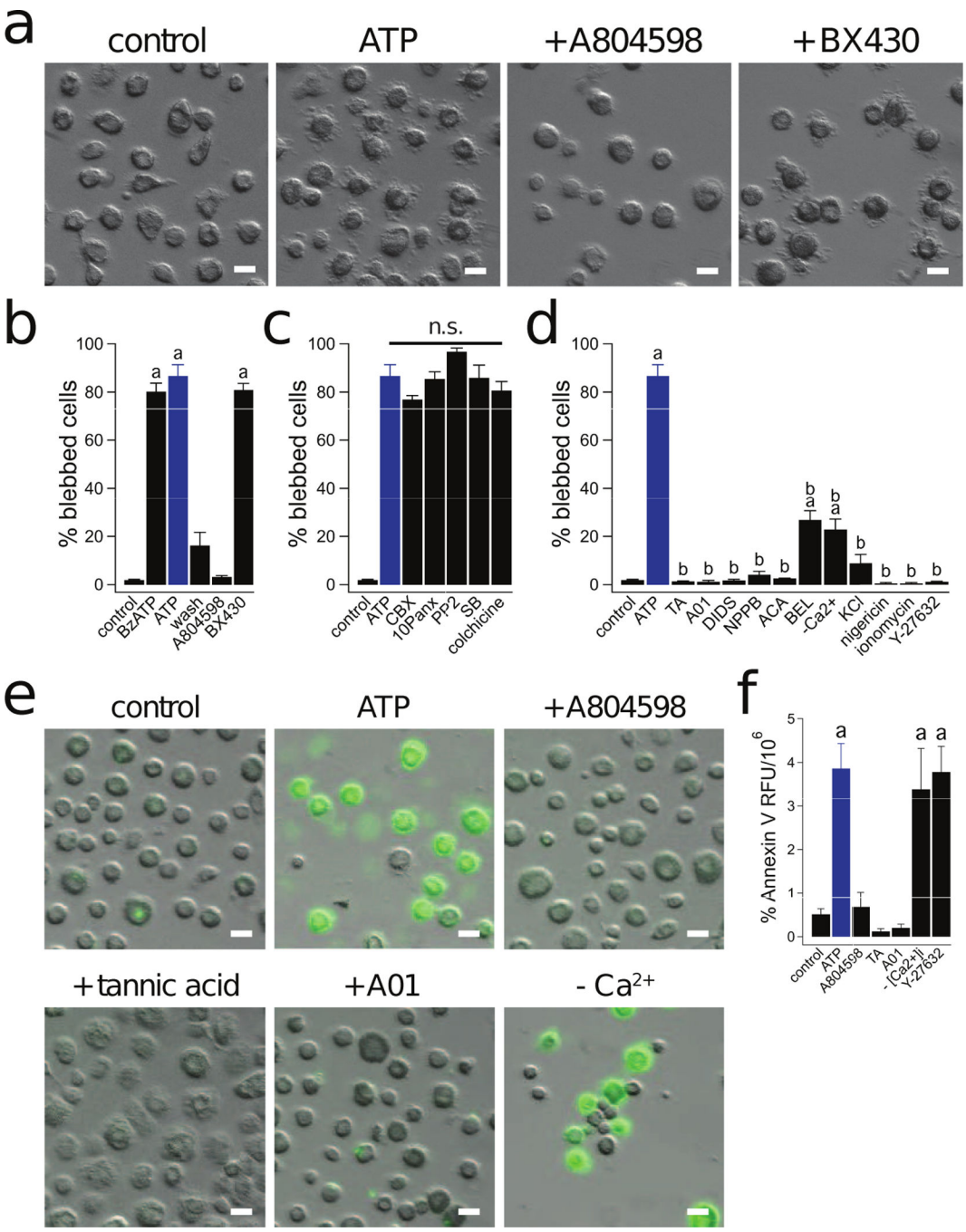

Figure 8. P2X7Rs drive macrophage blebbing.

(a) Macrophage blebbing induced by 15 min treatment with ATP (2 mM) +/− A804598 (1 μM) or BX430 (2 μM) at 37°C. **(b)** BzATP (300 μM) and ATP (2 mM) induced membrane blebbing. Note that the percentage of blebbed cells was significantly reduced after a 30 min washout of the ATP. Blebbing is prevented by A804598 (1 μM) but not BX430 (2 μM). “a” is significantly different from control ($p < 0.0001$, n = 4 experiments for each). **(c)** Preincubation of macrophages with CBX (20 μM), ^{10}panx (300 μM), PP2 (20 μM), SB (10 μM), or colchicine (50 μM) did not prevent ATP (2 mM) induced membrane blebbing. “n.s.”

denotes no significant difference. **(d)** The percentage of blebbed cells was significantly reduced by preincubation of macrophages with tannic acid (TA, 20 μM), A01 (40 μM), DIDS (100 μM), NPPB (100 μM), ACA (50 μM), BEL (50 μM), BAPTA (10 μM)/EDTA (1 mM) (-Ca^{2+}), ECS with 130 mM KCl, and Y-27632 (20 μM) ("b": $p < 0.0001$, $n = 5$ experiments each). Neither a 20 min stimulation of macrophages with nigericin (20 μM) nor ionomycin (1 μM) caused membrane blebbing (n= 4 experiments each). "a" indicates significant difference from control. "b" indicates significant difference from ATP. **(e)** Representative images of PS switch as measured by Annexin V fluorescence in macrophages treated with ATP (2 mM) +/− A804598 (1 μM), tannic acid (20 μM), A01 (40 μM), and BAPTA (10 μM)/EDTA (1 mM) (-Ca^{2+}) at 37°C. **(f)** ATP (2 mM) induced Annexin V RFU was significantly reduced by preincubation with A804598, tannic acid, and A01 ($p < 0.0001$, $n = 4$ experiments each), but not BAPTA/EDTA (-Ca^{2+}) or Y-27632 (20 μM) where "a" indicates significant difference from control. Scale bars: 20 μm.

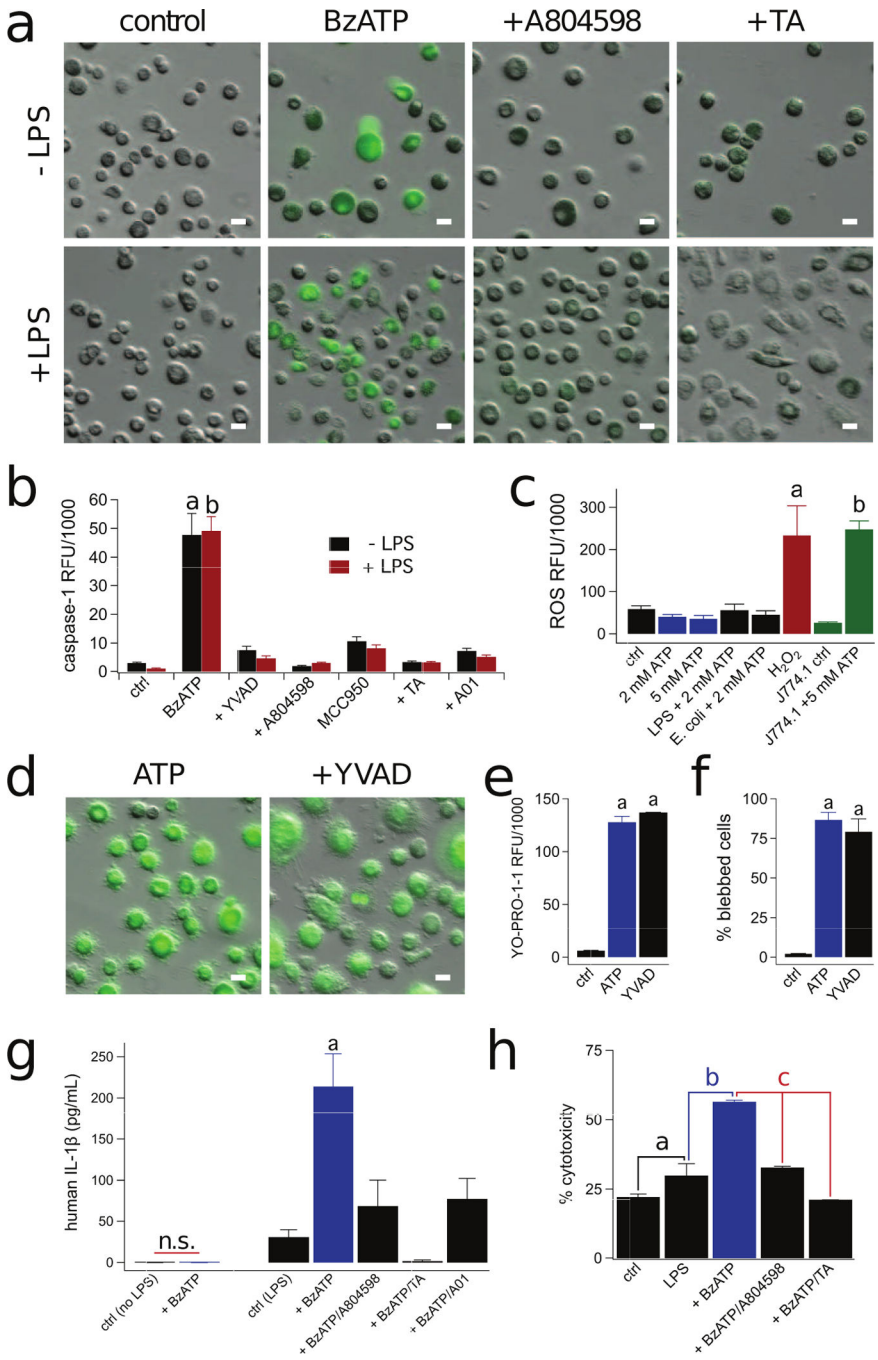

Figure 9. Macrophage P2X7Rs require Cl^- channels to activate caspase-1 and IL-1β release.

(a) Caspase-1 activation in macrophages treated or not with LPS (10 μg/mL, 3 hrs) and BzATP (300 μM) +/− A804598 (1 μM) or tannic acid (TA, 20 μM) for 30 min at 37°C. The increase in fluorescence (green) indicates activation of caspase-1. (**b**) Capase-1 was activated by BzATP (300 μM) in either LPS primed or unprimed macrophages. Significant reduction in caspase-1 activation by A804598 (1 μM), TA (20 μM), A01 (40 μM), YVAD (100 μM), and MCC950 (10 μM) ($p < 0.0001$, n= 6 experiments for each). “a” and “b” are significantly different from their respective controls. **(c)** Macrophage ROS production

measured after loading cells with DCF-DA for 30 min as the increase in DCF fluorescence. Human macrophages treated with ATP (2 mM) +/− LPS (10 μg/mL, 3 hrs), pHrodo Red *E. coli* BioParticles (40 μg/mL, 1 hr), or 5 mM ATP did not produce concentrations of ROS greater than untreated macrophages. Treatment with H_2O_2 (1 mM) was used as the positive control (n= 4 experiments each). J774A.1 mouse macrophages treated with ATP (5 mM) displayed significant ROS production ("b": $p < 0.0001$ unpaired t-test, n= 3 experiments). **(d)** Capase-1 inhibitor Ac-YVAD-cmk (YVAD, 100 μM), did not prevent YO-PRO-1 uptake **(e)** or blebbing **(f)** ("a": sig. difference between control $p < 0.0001$ unpaired t-test, n= 3 experiments). **(g)** Macrophages primed with LPS (10 μg/mL, 3 hrs) and stimulated with BzATP (300 μM) for 30 min at 37°C release IL-1β, and release is inhibited by pretreatment with A804598 (1 μM), TA (20 μM), and A01 (40 μM) $p < 0.001$ ANOVA, n= 6 experiments) "a": significant difference from control. (**h**) After LPS priming (10 μg/mL, 3 hrs), macrophages were treated with BzATP (300 μM) +/− A804598 (1 μM) or TA (20 μM) for 30 min at 37°C and supernatants were collected and LDH release was quantified; there was significant reduction by A804598 and TA ("c": $p < 0.0001$ ANOVA, n= 3 experiments). "a" indicates significant difference from control. "b" indicates significant difference from LPS. Scale bars: 20 μm.

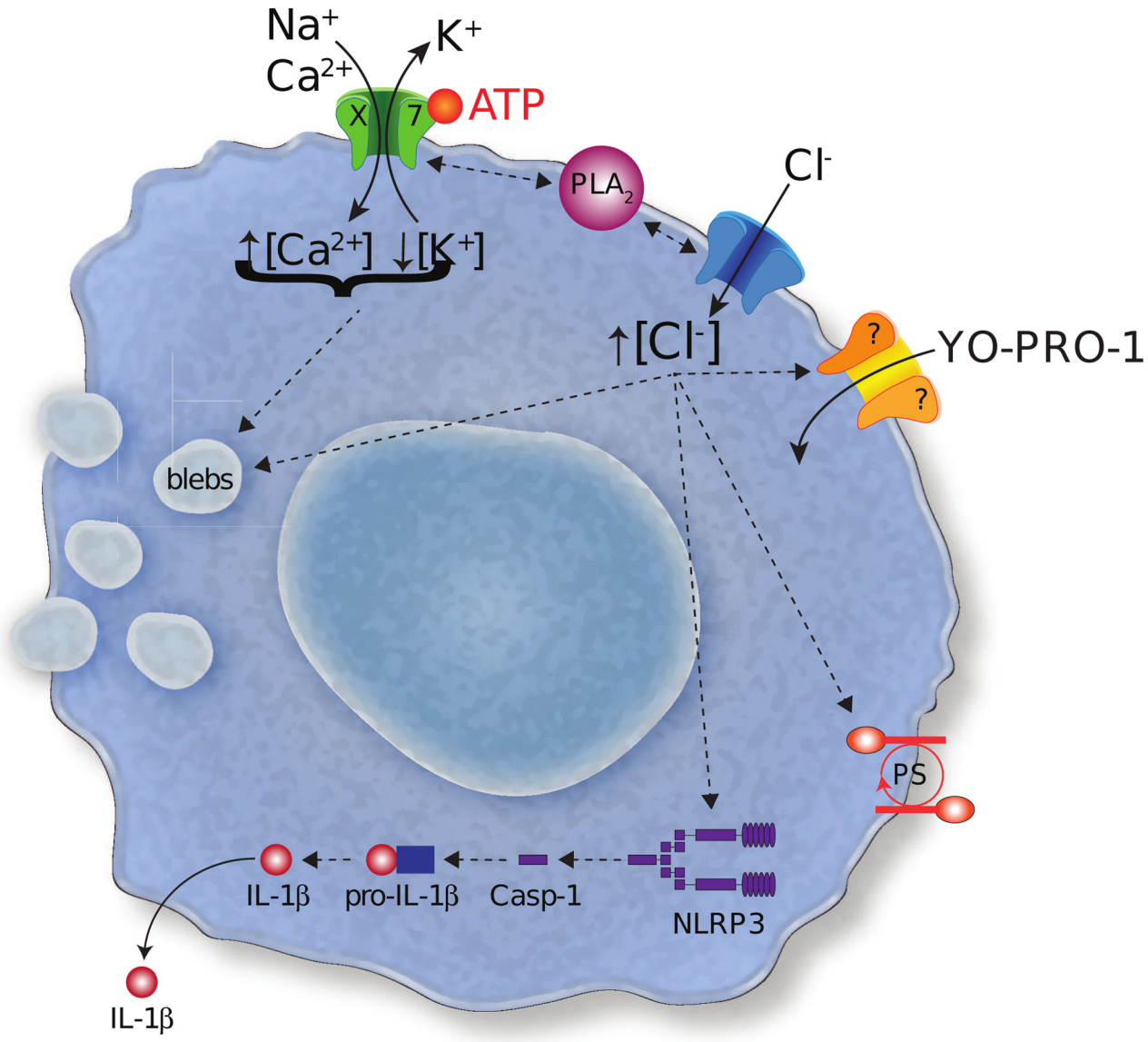

Figure 10. P2X7R pathways.

The cartoon shows the pathways suggested by the experiments outlined in the paper.